Safety and Environment Assessment of ARIES-AT

D. A. Petti, B. J. Merrill, R.L. Moore, G. R. Longhurst
Idaho National Engineering and Environmental Laboratory
Fusion Safety Program, P.O. Box 1625
Idaho Falls, ID 83415

L. El-Guebaly, E. Mogahed, D. Henderson, P.˚Wilson, and A. Abdou
Fusion Technology Institute
1500 Engineering Drive
University of Wisconsin-Madison
Madison, WI 53706

ABSTRACT

ARIES-AT is a 1000 MWe conceptual fusion power plant design with a very low projected cost of electricity. The design contains many innovative features to improve both the physics and engineering performance of the system. From the safety and environmental perspective, there is greater depth to the overall analysis than in past ARIES studies. For ARIES-AT, the overall spectrum of off-normal events to be examined has been broadened. They include conventional loss of coolant and loss of flow events, an ex-vessel loss of coolant, and in-vessel off-normal events that mobilize in-vessel inventories (e.g. tritium and tokamak dust) and bypass primary confinement such as a Loss of Vacuum and an in-vessel loss of coolant with bypass. This broader examination of accidents improves the robustness of the design from the safety perspective and gives additional confidence that the facility can meet the no-evacuation requirement. We also provide a systematic assessment of the design to address key safety functions such as confinement, decay heat removal, and chemical energy control. In the area of waste management, both the volume of the component and its hazard are used to classify the waste. In comparison to previous ARIES designs, the overall waste volume is less because of the compact design.

Safety and Environment Assessment of ARIES-AT

1. Background and Objectives

The DOE Fusion Safety Standard [1] was developed in 1996 to enumerate the safety requirements and to provide corresponding safety guidance related to the hazards associated with D-T magnetic fusion facilities. Furthermore, from a regulatory perspective the standard also establishes the design and operational envelopes for fusion facilities.

The highest level requirements in the Fusion Safety Standard [1] stem from DOE policy, namely:

- The public shall be protected such that no individual bears significant additional risk to health and safety from the operation of those facilities above the risks to which members of the general population are normally exposed.
- Fusion facility workers shall be protected such that the risks to which they are exposed at a fusion facility are no greater than those to which they would be exposed at a comparable industrial facility.
- Risks both to the public and the workers shall be maintained as low as reasonably achievable (ALARA).

In addition to these requirements, two additional fusion-specific requirements were developed in the standard [1]:

- The need for an off-site evacuation plan shall be avoided
- Wastes, especially high-level radioactive wastes, shall be minimized

The ARIES program has adopted these last two requirements for their design studies. These stringent requirements have specific impacts in terms of materials selection and design decisions and were adopted to demonstrate the safety and environmental potential of fusion

power. In terms of the no-evacuation requirement, a dose limit of 10 mSv (1 rem) in a worst case accident is recommended in the DOE Fusion Safety Standard consistent with current guidance from the Environmental Protection Agency. The waste minimization requirement is currently interpreted in the ARIES context as generating as small a volume of waste as possible and requiring that all waste be able to disposed of as low-level waste (Class C or better). In addition, effort is made to try to select materials (and their associated impurity level) to allow for the potential of recycling of the activated material in either a hands-on or remote (shielded) mode.

In the following sections, we evaluate the ARIES-AT design against these requirements. Section 2 discusses the radiological inventories and release limits that must be met by the design. Section 3 assesses the implementation of safety in the ARIES-AT design by examining the key safety functions in the facility and a set of select associated accidents that could challenge the functions under an off-normal condition. A characterization of the hazard and volume of waste produced from ARIES-AT at the end of its life is the subject of Section 4.

2. Radiological Inventories and Release Limits

2.1 Radiological Inventories

The major radiological inventories in the ARIES-AT design are tritium and activation products in plasma facing components, in structural materials and in the coolant. Section 2.1 discusses the major tritium inventories in the ARIES-AT and Section 2.2 discusses the neutron activation in the components. Of greatest concern are those inventories that can be mobilized in an accident. These include tritium, tungsten dust, and Hg-203 and Po-210 in the LiPb. As shown in Section 3, structural temperatures remain low enough during accidents (< 800¡C) that release of activated structure via oxidation driven mobilization is not a serious concern.

2.1.1 Tritium. Tritium is found in three major locations in the in-vessel components in the ARIES-AT: in the W plasma facing components in the divertor, in the LiPb coolant, and in the SiC structure. The amount of tritium in the W armor of the divertor is small. Analysis of the inventory of implanted tritium in the tungsten [2] is on the order of 0.4 g/m^2. With a divertor area of 135 m^2, this surface coverage translates into ~ 54 g of tritium. In addition, about ~1-2 g of tritium are bred in the SiC in the divertor via nuclear reactions. Thus, the total inventory in the divertor is ~ 30 g.

Tritium in the LiPb coolant is extremely small (< 1 g) because of the very low solubility of tritium in LiPb. The rather low solubility results in a partial pressure of tritium over the LiPb of about 20 Pa. In this case permeation is a concern and the tritium must be recovered from the gas phase to minimize permeation into the secondary coolant (helium).

Tritium in the first wall and SiC comes from implantation/uptake from the plasma and production via nuclear reactions in the SiC. Analysis of tritium uptake in the plasma chamber indicates ~ 534 g in the first wall and ~ 150 g could be formed as co-deposited layers in the vacuum vessel due to sputtering of the SiC and subsequent C:H re-deposition in cooler regions of the plasma chamber such as the pumping ducts [2]. In addition, nuclear reactions are expected to generate ~ 7 g of tritium in the SiC structure. The overall inventories are summarized in Table 1.

Of these inventories, the major source of mobilizable tritium would be from the co-deposited layer [2]. The greatest concern would be the levitation of this material and its potential for being carried to the surroundings in the event of a breach of the vacuum vessel confinement boundary. The fraction of tritium released would depend on the location of the break relative to the location of the co-deposition. In some machines, the co-deposited material is flaky and easily mobilizable. In other cases, the material is tightly bound to structure as a carbonaceous or polymer-like film. We assume in the analysis presented here that the entire

150 g of co-deposited tritium is mobilized in any event in which the vacuum vessel is breach. In addition to the co-deposited material, the tritium in the tungsten divertor plate will come out at a fairly high rate even if the plates are at ambient temperature. Thus, an additional 55 g is considered to be mobilizable in an accident.

The bulk of the tritium in the SiC is tightly held in the SiC matrix under the accidents considered in Section 3. The low diffusivity in the SiC results in very little release in accidents. For example, after one year at 750¡C only 6% of the tritium is released [2]. Much higher temperatures (in excess of 1400¡C) would be required to mobilize this inventory. No accidents have been identified in the ARIES-AT design that could result in a temperature of 1400¡C in SiC (see Section 3).

2.1.2 Neutron Activation

2.1.2.1. Introduction. Detailed activation calculations for ARIES-AT are performed to evaluate the safety aspects of the plant. A detailed discussion of the activity results for various device components and the radiological inventory assessment of the LiPb coolant/breeder are provided in this section. As will be discussed later in Section 3.3, the activation results are used to generate the decay heat distribution throughout the device in order to determine whether a LOCA or LOFA is the critical accident event. Furthermore, in section 4, the activation results will be used to evaluate the hazard of ARIES-AT components and their ultimate disposition as waste.

The ARIES-AT machine has a lifetime design of 40 full power years (FPY), which except for the first wall, is also the lifetime of most components. The plasma facing components must be replaced after 4 FPY because of the damage caused by the high neutron wall loading. The average inboard (IB), outboard (OB), and divertor wall loadings are 2.3, 4.1, and 1 MW/m^2, respectively. The operation schedule of the facility consists of a ~10-month steady-state operational period followed by a two-month extended maintenance period, resulting in an 80% availability for the facility.

2.1.2.2. Computational Model. The ARIES-AT radial builds for the activation calculations and the constituent material compositions for the various components used in the analysis are provided in Reference [3]. Impurities for all materials included in the analysis are listed in Table 2. The IB high-temperature (HT) shield and OB blanket-II contain the W stabilizing shells required for plasma control. The IB side vacuum vessel (VV) employs tungsten carbide (WC) filler to reduce the radial standoff.

The neutron flux throughout the facility was computed using the FENDL-2 175 neutron 42 gamma group coupled cross section library [4] and the DANTSYS [5] discrete ordinates, deterministic transport code. Note that the 1-D analysis tends to overestimate the flux at the plasma facing components in particular. To compensate for the overestimation, the more accurate fluxes of the 3-D analysis were used to re-normalize the neutron source for the individual components in the 1-D activation calculations. For the activation analysis, use is made of the ALARA activation code [6], the most recent activation code developed at the Fusion Technology Institute at the University of Wisconsin. The FENDL-2 175-neutron group transmutation cross-section library is employed for these calculations [7].

2.1.2.3. Activity Analysis. The specific activity results for the inboard, outboard, and divertor components of ARIES-AT are depicted in Figures 1, 2 and 3 for the fully compacted solids of ARIES-AT. One notes immediately that the IB and OB FW/Blanket-I have the highest activity at shutdown. The activity drops by nearly two orders of magnitude below the level of the ferritic steel components after a one-hour shutdown and by three orders of magnitude over the course of a day. This drop in activity is due to the decay of the short half-life (< 10 min) radionuclides ^{28}Al and ^{27}Mg and the radionuclide ^{31}Si (2.62 hr half-life), that are generated in the SiC structure of the FW/Blanket-I components. The activity level of the vacuum vessel eventually drops to the level of the SiC-containing FW/Blanket-I components 10-100 years after shutdown of the device. The activity of the OB blanket-II component containing the W stabilizing shells remains fairly level for several weeks before dropping nearly one order of magnitude one

year after shutdown of the facility. Its activity reaches levels comparable to that of the SiC containing FW/Blanket-I structures 5-6 years after shutdown. The dominant radionuclides for several major components are listed in Table 3 at various times after shutdown.

Another interesting feature to note in Figs. 1 and 2 is a comparison of the activity of the HT shield and vacuum vessel for the inboard and outboard components. For the inboard components the HT shield and the VV have approximately the same activity level at shutdown until about a week after shutdown. Thereafter, the activity of the VV drops below that of the HT shield. The high initial activity level in both components is due to the presence of tungsten in each component. Recall that the VV has a WC filler and the HT shield contains tungsten stabilizing shells. The activity of the W stabilizing shells is quite high and it is the main contributor to the overall activity of the HT shield immediately after shutdown. After 30 days to half a year, ^{55}Fe begins to dominate the activity of the HT shield. The half-life of ^{55}Fe is much longer than that of several of the short-lived tungsten radionuclides (^{185}W and ^{187}W). The situation is different on the outboard side of the machine. Here the VV is mainly comprised of 70% water and 30% structural steel. The water moderates the high energy neutrons to lower energies creating a high thermal neutron peak compared to the remainder of the neutron spectrum (3 orders of magnitude higher thermal flux). Hence, the thermal neutron absorption by iron, chromium and nickel leads to a higher activity of the VV structure than the HT shield.

2.1.2.4. Radiological Inventory Assessment of LiPb. The activation and subsequent decay heat and radiological analyses of LiPb coolant/breeder are more complex than that of the other major components. This is because it circulates in and out of the neutron radiation field in five separate coolant flow paths through the device [8]. Each channel carries a portion of the coolant through a sequence of different structural components, each having a different residence time. The LiPb is modeled by considering a given control volume as it circulates through the system. The irradiation history of the control volume can be represented as a pulsed history with one pulse for each pass through the flow channels. The fluence that a given

control volume of LiPb receives is a function of the flux spectrum and residence time of the flow path it follows. Several flow paths are modeled with residence times ranging from 1 to 240 s. Finally, the flows from the different flow paths spend approximately two minutes outside the blanket region and mix in various sub-systems (e.g. heat transfer, chemistry control). In the actual design, a given control volume does not necessarily follow the same flow path each time through the device.

Three approximations were used in an attempt to simulate these effects. The first approximation (EU Approx) is based on the method used by the Europeans [9]. In this most simple approximation the activation response is calculated for 40 FPY at a single point, the outboard first-wall, and divides this response by 10 to approximate all the effects of system availability, residence time, spatial variation and ex-vessel mixing.

The second approximation (Approx 1) is slightly more sophisticated. In this approximation, the activation responses for the entire LiPb system are calculated using an average residence time of 80 s and an average ex-vessel time of 120 s. The approach explicitly includes the effects of system availability, flow history pulsing (through an average residence time), and the geometric distribution of the neutron flux. It does not include the effects of the variation in flow history among the different flow paths, nor of the sequence of components through which each control volume passes within a flow path. Finally, and perhaps most importantly, it does not include the effects of ex-vessel mixing of the various flow paths.

The final approximation (Approx 2) improves on the previous one by simulating the exact residence time in each component. For this approximation, the components that experience each of the different residence times are modeled in separate invocations of ALARA for each point in the operating history. Thus, a control volume of coolant that spends 10 s in the first wall followed by 80 s in the blanket channel, will be modeled by two control volumes, one repeatedly spending 10 s in the first wall and the other repeatedly spending 90 s in the blanket

channel, both spending 120 s in the ex-vessel system. This approximation still has the same shortcoming of the previous approximation, namely the lack of ex-vessel mixing.

The radiological hazardous material inventory in LiPb was modeled using the complex irradiation history outlined above. The primary radiological concern for LiPb is from the radionuclides ^{210}Po and ^{203}Hg. Both of these isotopes have well defined primary production pathways beginning with the Pb isotopes ^{206}Pb and ^{208}Pb:

$$^{208}\text{Pb} \xrightarrow{(n,\gamma)} {}^{209}\text{Pb} \xrightarrow{(\beta^-[3.25h])} {}^{209}\text{Bi} \xrightarrow{(n,\gamma)} {}^{210}\text{Bi} \xrightarrow{(\beta^-[5.01d])} {}^{210}\text{Po},$$

and $^{206}\text{Pb} \xrightarrow{(n,\alpha)} {}^{203}\text{Hg}$.

In addition to ^{208}Pb and ^{206}Pb, the LiPb coolant contains a 43 wppm impurity of ^{209}Bi and that is a two-step neutron absorption and subsequent decay process leading to ^{210}Po. A number of longer Pb based pathways also contribute to the ^{203}Hg concentration over the lifetime of the coolant.

Figure 4 shows the inventories of ^{209}Bi and ^{210}Po in the full 600 m^3 volume of the LiPb coolant for all three approximations. Note that the Approx 1 and 2 results agree well within 10%, indicating that the simpler Approx 1 method could be used in future analysis without introducing large error to the final results. The EU approximation overestimates the Po and Bi inventories, meaning the OB FW flux and spectrum are not representative. The high FW flux accentuates the double capture process that lead to high ^{210}Po production. Furthermore, the LiPb coolant has a ^{209}Bi inventory > 10% of that of the OB FW.

The ^{209}Bi inventory is of interest because, as a precursor to ^{210}Po, control of its concentration can serve as a mechanism to limit the ^{210}Po inventory. The 43 wppm Bi impurity dominates the ^{210}Po production at the early years of operation (60% @ 4 FPY) while the contribution from Pb is dominant (85%) near the end of operation. It is clear from this figure that the ^{210}Po levels are above the radiological release limit of 25 Ci for ^{210}Po (discussed in the next section) very soon in the operational life of the facility, primarily due to the initial bismuth

impurity. A purification system is therefore necessary to remove the ^{210}Po [10] generated by Pb and Bi during operation. Figure 5 displays the activity of ^{203}Hg over the lifetime of the facility. Note that after a few days the activity is above the radiological release limit of 25 kCi for ^{203}Hg (discussed in the next section) and a purification system will be necessary to control its level.

Based on these results, the isotopes of specific interest to the safety assessment are the Po-210 and Hg-203 in the LiPb coolant and the activated tungsten divertor plate, which could produce tungsten dust via a disruption. For the safety assessment, inventories in the coolant have been estimated based on an estimated residence time of the LiPb in each circuit and assuming conservatively cleanup of the bismuth in the coolant to 1 ppm [11]. (The results from Reference 10 suggest much better removal is possible.) This results in about 0.1 ppb of Po-210 in the coolant. The results are shown in the Table 4. (If there were no cleanup of bismuth and Po-210 in the coolant then the Po-210 inventory would be 190 kCi.) The specific activities of the dose-dominant isotopes in tungsten are shown in Table 5.

2.2 Allowable Releases

Radiological release targets for tritium, activated tungsten (e.g. tokamak dust), Hg-203 and Po-210 have been established to meet the 10 mSv (1 Rem) no-evacuation limit. Radiological dose calculations have been performed using the MACCS2 code for radionuclide release from a 100-m stack and at ground level for a 1-km site boundary. Dose-to-release values were calculated using meteorological conditions representative of the Idaho National Engineering and Environmental Laboratory, a large DOE site assuming Pasquill-Gifford dispersion. [12] Given the best-estimate nature of no-evacuation assessments, average weather conditions (stability class D and wind speed 4 m/s) were used. Based on these

calculations, allowable releases in curies for the safety-important isotopes were established. [a] Results are shown in Table 6. In the case of tungsten dust, the radionuclide inventories of the predominant tungsten, hafnium and rhenium isotopes produced in the tungsten were combined with the allowable release for each isotope to obtain a release target for dust in terms of total mass. Results for tritium are assuming the HTO form. Ground level release limits are used because most of the accidents identified in Section 3 result in releases that do not go up the stack.

As shown in Table 7, by comparing the mobilizable inventories with these limits, we can determine the degree of radiological confinement that we need during accidents to meet the no-evacuation limit. A factor of only 20% confinement is needed in tritium, approximately a factor of 10 for tungsten dust and a factor of 50 to 100 for events in which Hg-203 and Po-210 are mobilized from the LiPb coolant.

3. Assessment of Safety Implementation in Design

3.1 Introduction

Because of the use of tritium and the presence of activated materials in AREIS-AT, some degree of radiological confinement is needed to protect the public and the workers at the facility. In keeping with the philosophy outlined the DOE Fusion Safety Standard, radiological confinement is implemented as the key safety function in ARIES-AT. Radiological confinement is implemented to ensure that releases during normal operation are kept as low as reasonably achievable and that releases during accidents are below the no-evacuation release limits discussed in Section 2.

[a] More recent DOE rules require that worst case meteorology should be used. This would results in release limits that are ten times more restrictive than in Table 4. The safety analysis results presented later in this paper indicate that ARIES-AT can still meet the no-evacuation limit of 10 mSv under worst case weather if isolation of HVAC systems occurs in 30 minutes instead of one hour or if Po and Hg inventories can be reduced by 50% reliable to the conservative levels assumed here via on-line removal .

Double confinement is implemented in ARIES-AT around all of the large inventories of tritium and activation products. For in-vessel inventories, the vacuum vessel and its extensions are the primary confinement, and the cryostat and its extensions are the second confinement boundary. In the heat transfer systems, the coolant piping forms the primary boundary and the vaults or rooms that house the coolant systems form the second boundary.

Demonstration of compliance with the no-evacuation safety requirements [1] requires examination of a broad range accidents that could challenge these radiological confinement boundaries to determine if any could lead to releases in excess of the no-evacuation limits. These accidents fall into three major categories:

- events that directly breach a confinement boundary (e.g. loss of vacuum, overpressure failure of the vacuum vessel, in-vessel loss of coolant with bypass of vacuum vessel),
- events related to decay heat removal (e.g., complete loss of coolant or loss of flow), and
- events associated with the chemical reactivity of materials (e.g., ex-vessel spill of LiPb coolant).

In the following sections, an overview of each these events is provided, followed by a detailed analysis of the progression of the accident including the accident's consequences in terms of releases to the environment.

3.2 Challenges to Radiological Confinement

The major challenges to radiological confinement fall into two main categories: a loss of vacuum event induced by failure of the confinement boundary and in-vessel coolant breaches that result in overpressure and subsequent failure of the confinement boundaries.

3.2.1 Loss of Vacuum Event (LOVA). In this event it is assumed that the two confinement barriers surrounding the tokamak (VV and its penetrations and cryostat and its

penetrations) fail at some point (most likely at a penetration) allowing air to enter the plasma chamber. The ingress air would instantly extinguish the plasma and cause a density-limit disruption that would mobilize some dust (probably tungsten from the divertor). Plasma control in ARIES-AT is expected to be good enough to prevent any significant erosion of plasma facing materials. However, the air ingress is expected to cause a disruption that based on ITER estimates [13] could mobilize 10 kg of tungsten in the divertor with a diameter of 0.1 microns depending on the magnitude of the disruption and the surface area of the divertor affected. The 205 g of easily mobilizable tritium (corresponding to 1.37 kg of HTO) would also become airborne in the plasma chamber. The mobilization time is 100 s, which corresponds approximately to the time required for the vacuum vessel to pressurize during the LOVA.

Based on loss of vacuum experiments in Japan [14], air exchange between the plasma chamber and the room containing the air would continue unimpeded. The flow is driven by the density gradient between the hot air inside the plasma chamber (heated by convection from the hot in-vessel components) and the cooler air surrounding the tokamak. This flow would eventually decrease to a level consistent with the equilibrium temperature of the in-vessel components (following their cooldown) and the outside environment. Releases to the environment would depend on the filtration and ventilation system in the room associated with the break. For the ARIES-AT LiPb/SiC blanket, the air ingress could also lead to oxidation of the SiC. Three different potential reactions have been considered:

$$SiC + 0.5\ O_2 = CO + Si$$

$$SiC + O_2 = CO_2 + Si$$

$$SiC + O_2 = SiO_2 + C$$

The third reaction has the greatest free energy of formation and thus is expected to dominate. Some CO and CO_2 would be produced but the quantities would be quite small.

Since the SiO_2 is a glass, it is expected to be a protective oxide layer, impeding the overall oxidation. Thus, this LOVA is not expected to involve any of the chemical energy sources in the blanket.

To analyze this event, a MELCOR model[b] of the ARIES-AT design was developed [15,16]. The model includes: 1) the free volume within the vacuum vessel (VV) and pumping ducts, 2) the in-vessel first wall (FW), high temperature shield (HTS), and divertor plate (DP) components, 3) the VV walls, 4) the confinement building upper functional areas (UFA), the heating-ventilation-air-conditioning (HVAC) system of the UFA, and 5) a duct that connects the VV to the UFA. The free volume in the VV and pumping ducts was estimated to be 785 m^3, of which 425 m^3 is the plasma chamber volume. The in-vessel plasma facing components (PFCs) were modeled as either SiC or tungsten walls (areas of 425 m^2, 135 m^2, and 230 m^2 for the FW, DP, and the portion of the HTS behind the divertor, respectively). The coolant side temperatures of the PFCs linearly drop from 1100¡C to the 650¡C (inlet coolant temperature) within 60 seconds of the initiation of the LOVA, then continues to drop at a rate of 30¡C per hour until a minimum coolant temperature of 350¡C is reached. The VV walls (850 m^2) were maintained at 75¡C over the duration of the event.

The UFA is assumed to be interconnected, having a total volume of 5880 m^3 (29 m x 29 m x 7 m), and located at ground level elevation. The bypass duct that connects the VV to the UFA is assumed to have a cross-sectional area of 0.02 m^2 (diameter of 0.16 m), and a length of 10 m. The size of the duct has been selected to simulate a diagnostic or heating port in the VV. Because the UFA are non-nuclear rooms of the confinement building, the HVAC air exchange rate of one volume per hour and a leak rate of one volume per day at an overpressure of 400 Pa were assumed for the UFA. These specifications are based on the ITER design of rooms

[b] MELCOR is being developed at the Sandia National Laboratory (SNLA) to analyses severe accidents in fission reactors. MELCOR tracks the flow of two-phase water during such accidents, as well as any radioactive aerosols that may exist in either fluid phase. Structure temperatures are determined by one-dimensional heat conduction equation solutions. Heat transfer to both phases is considered. External (walls) or internal (pipes) flow configurations are simulated during force, natural, boiling, and condensation heat transfer modes. Modifications have been made to MELCOR at the INEEL for fusion specific analyses.

around the tokamak.[c] The bypass duct was divided vertically into two flow paths to allow for the prediction of a counter-current flow pattern expected to develop within this duct due natural convection during this event. The HVAC is assumed to turn off after one hour, isolating the UFA, and a VV detritiation system starts that circulates one VV volume per hour. These assumptions are similar to those developed for the ITER EDA safety study.[13]

Figure 6 contains the predicted vacuum vessel pressure during this event. The pressure in the vacuum vessel reaches a near equilibrium with the UFA in about 500 seconds. Figure 7, which contains the predicted flow in the bypass duct, shows that equilibrium between these two volumes does not actually occur until later in the event. Although not easily seen, outflow from the VV does not occur until almost 2000 seconds. Initially the flow is into the VV at a rate of 3.4 kg/s. This flow is choked until about 70 seconds. Figure 8 shows that the flow in the duct becomes stratified beyond 2000 seconds at about 5 g/s. The inlet flow being slightly larger because the air temperature in the VV drops as the internal components of ARIES-AT cool. When this cooling stops, the flows in the duct equilibrate at about 2 g/s, which is a flow velocity of about 0.5 m/s. Figure 9 presents the mass of tungsten dust in the UFA during the first two hours of the LOVA. Also included in this figure is the amount of dust stacked to the environment by way of the HVAC system. As can be seen, only about 0.15 g of dust makes it to the UFA, of which 0.04 g is released to the environment before the UFA is isolated. The reason for this low release is that most of the dust in the VV settles to the floor of the VV before outflow from the VV begins, that is only 270 g of the initial 10 kg remains airborne by 2000 seconds. In addition to the dust release, an estimated 0.07 g of HTO is stacked by way of the HVAC system during the first hour of the event, with an another 0.02 g leaked from the UFA over the course of a day.

There is some uncertainty regarding the initial inventory of dust in the VV, which could be as high as 110 kg based on detailed analysis for ITER. However, because this release

[c] This leak rate is less than the confinement buildings of some DOE reactors but much higher than fission reactor containment buildings.

scales almost linearly with initial mass mobilized, it is expected that the release from 110 kg of tungsten dust would be small as well. A summary of the source term behavior for this event is found in Table 8.

3.2.2. In-vessel LOCA. Since the LiPb blanket coolant is not significantly pressurized and will not change phase upon pipe breach, an in-vessel blanket LOCA does not generate any significant pressure. However, the low temperature shield/vacuum vessel is cooled with pressurized water. Accommodations such as a suppression system or an expansion tank with a passive rupture disk are needed to ensure that the plasma chamber is not overpressurized in the event of a LOCA of this system.

In this event, it is assumed that there is a small in-vessel LOCA associated with failure of the water-cooled low temperature shield/VV. The size of the break is approximately 4.5 cm in diameter. The in-vessel LOCA is assumed to cause a plasma disruption and terminate the plasma. The pressurized water from the break then sprays onto the back of the LiPb/SiC blanket where it enters film boiling. The steam that is generated is superheated because of the high temperatures of the in-vessel components and thus rapidly pressurizes the vacuum vessel. The overpressure in the vacuum vessel is assumed to fail a penetration and cause a bypass of confinement. The pressure suppression system is assumed to open at a pressure of 0.2˚MPa (2 atm) in the vacuum vessel. The impingement of water from the low temperature shield onto the back of high temperature shield will probably cause the high temperature shield to fail because of thermal stress or cracking of the SiC or the formation of SiO_2. LiPb would be released from the failed blanket sector and puddle on the floor of the vacuum vessel. The pool will fill up half of the plasma chamber to a depth of ~ 3.25 m. Because all of the in-vessel surfaces of ARIES-AT are above the critical temperature of water, any water released from the break will flash to steam and become superheated. Thus, no interaction between water and the LiPb pool is expected. However, the LiPb pool is expected to release any Po-210 and Hg as it cools at the bottom of the vacuum vessel.

To analyze the in-vessel LOCA between the vacuum vessel and plasma chamber with an additional bypass break between the plasma chamber and the upper functional area (UFA), the MELCOR model developed for the LOVA event was modified and expanded. The modifications and expansions are described next.

The MELCOR code was developed to use only one system coolant. In the case of ARIES-AT the first wall and blanket regions (FW/B) are cooled by four LiPb (Lithium-Lead) loops and the vacuum vessel structure that encloses the FW/B region is cooled by a high-pressure water loop. In order to model two different coolants in the same MELCOR model, the LiPb coolant in the FW/B region was simulated using heat structures. Control functions were used to model the advective and convection heat transfer in the coolant (heat structures) and from the coolant (heat structures) to the flow channel walls respectively. The remaining portions of the loop (piping and heat exchanger) were not modeled. Thus, the inlet temperature of the LiPb to the FW/Blanket region was assumed to be a constant 932 K.

The vacuum vessel (VV) model was expanded to include the coolant loop as well as the structural walls. It was assumed that the low temperature shield/vacuum vessel coolant loop was similar to the VV coolant loop used for ITER. The ITER volumes and surface areas were scaled to those corresponding to ARIES-AT design. This resulted in a loop containing approximately 94000 kg of water at an initial pressure of 1.87 MPa and a temperature of 350 K.

The bypass model is the same as used for the LOVA analysis. Thus, the bypass duct that connects the VV to the UFA is assumed to have a cross-sectional area of 0.02 m^2, and a length of 10 m. The duct simulates a diagnostic or heating port in the VV that is postulated to break due to the high pressure that develops in the plasma chamber during the LOCA. The bypass duct is divided into two flow paths to allow for the counter current flow that may develop within the duct due to natural convection. The heating-ventilation-air-conditioning system is assumed to function the same as in the LOFA event.

A suppression system similar to the one designed for ITER is needed to relieve the pressure in the plasma chamber in the event of a LOCA. The suppression system consists of piping connecting the reactor to a 2250 m^3 suppression tank containing 1045 m^3 of saturated water (pressure = 2300 Pa). The piping contains a passive rupture disk that will open when the pressure differential across the rupture disk exceeds 0.2 MPa. The suppression system used in this analysis is not optimized for the ARIES-AT design however it does show that a suppression system will keep the plasma chamber pressure below its design limit in the event of a small in-vessel LOCA.

The in-vessel LOCA is assumed to cause a plasma disruption and terminate the plasma burn. The pressurized water (initial pressure = 1.84 MPa) from the break sprays onto the back of the hot HTS where it enters film boiling. The steam that is generated from flashing and film boiling is superheated because of the high temperatures of the in-vessel components and thus rapidly pressurizes the plasma chamber. The pressure in the plasma chamber (see Figure 10) increased from an initial 500 Pa to a maximum pressure of 0.26 MPa in 60 seconds. The pressure in the plasma chamber peaks at 0.26 MPa because the suppression system rupture disk opens at a pressure of 0.2 MPa (2 atm), approximately 10 seconds after the break. The opening of the suppression system results in the high-pressure steam flowing to the suppression tank where it is condensed in the pool of subcooled water contained in the suppression tank. As shown in Figure 11, all the flow from the break is converted to steam during the first 500 seconds of the transient. At 500 seconds, a small amount of water begins to collect at the bottom of the plasma chamber where it remains in film boiling for ~ 3500 seconds as indicated by the accumulated liquid mass curve in Figure 11.

Although the pressure suppression system opens at 0.2 MPa, the peak pressure in the vessel reaches ~ 0.26 MPa. This high pressure is assumed to cause a failure in a duct that connects the VV to the UFA causing a bypass of the confinement. As shown Figure 12, mass exchange occurs between the plasma chamber and the UFA room during the first 500 seconds

of the event. At ~ 500 seconds the flow reverses. Thus, the flow is now from the UFA room to the plasma chamber (both in the upper and lower portion of the duct) due to the pumping action of the suppression system keeping the pressure of the plasma chamber slightly below atmospheric pressure. These results show that radiological release to the environment can only occur during the first 500 seconds of the accident. During this time period (as shown in Figure 13) most of the flow from the plasma chamber is to the suppression tank.

The source terms for this event includes the 205 g of mobilizable tritium in the vessel, 10 kg of tungsten dust generated from the disruption, and the release of Po-210 and Hg from the LiPb pool on the floor of the plasma chamber. The overall releases to the environment from this accident are shown in Table 9. The results show that the pressure suppression system is quite effective at capturing most of the material that is mobilized in the plasma chamber. Thus, the releases are small and well below the no-evacuation limits.

3.3. Decay Heat Removal

A series of complete loss of coolant accident (LOCA) and total loss of flow accident (LOFA) were analyzed for ARIES-AT to examine the ability to passively remove decay heat form the machine. The high initial activity of the SiC first wall component translates directly into the initial high decay heat of the first wall components. The time dependent behavior of the decay heat for various components during the time period of interest (one week) is depicted in Figures 14, 15, and 16 for fully compacted components. Note that the initial high decay heat of the first wall components drops to levels below that of the ferritic steel components within 20 minutes to one day after shutdown of the facility. This means that SiC contributes to the initial heat load after a LOCA/LOFA event and that the long-term heat sources are the steel and W components. The IB and OB segments of the VV generate higher decay heat compared to the HT shield due to the higher initial activity of the VV. Table 10 lists the dominant radionuclides in descending order for the major components.

The effect of the LiPb decay heat on a LOCA and LOFA must be analyzed to determine which accident event is the more limiting from a decay heat removal standpoint for the facility. Figure 17 compares the decay heat of the LiPb (without tritium) and OB FW/Blanket structure. Note that the initial decay heat loading of the OB blanket region is driven by the SiC containing FW structure. As noted earlier, this is due to the high initial activity of the SiC components. Within one hour after shutdown, the decay heat of the FW/Blanket-I structure drops to the same level as that of LiPb. The decay heat of LiPb exceeds that of the FW/Blanket structure in the time frame of several hours to weeks after an accident meaning that the dominant energy source during this period in the blanket region is LiPb. Thus, because the heat load to the structure is higher in the LOFA than in the LOCA, the LOFA event is more limiting.

There is a large difference between the time scale of plasma shutdown (¯1 ms) and the loss of coolant or loss of flow (several minutes-hours). Thus, the plasma is assumed to be immediately quenched at the onset of the LOCA/LOFA and the chamber components temperature begins to increase due to the decay heat generated. The initial temperature of different reactor components used in this study is listed in Table 11. The base case assumptions are:

- Adiabatic boundary conditions at the inner surface of the inboard vacuum vessel (I/B VV).
- The outer surface of the outboard vacuum vessel (O/B VV) radiates to the gate of the maintenance port.
- The maintenance port convects (naturally) to the atmosphere at 20¡C (ultimate heat sink).
- Thermal radiation is allowed in the gaps between surfaces.
- Emmissivity is 0.5.

An axisymmetric finite-element model in the r-z plane was constructed to analyze these events. Assuming symmetry, the analysis was done for the upper half only; the divertor region

and tungsten shells are included. This model assumes complete symmetry around the vertical z-axis. The ANSYS 5.4 code is used to perform this analysis [17]. Figure 18 shows the 2-D axisymmetric finite-element model used in this analysis.

The activation analysis determines the time dependent thermal load to the individual elements of each component. The detailed time-dependent and material-specific decay heat loads are used with the boundary conditions and the initial temperatures for various ARIES-AT components to determine the thermal performance of the reactor. The transient thermal analysis is performed for the upper half model of ARIES-AT for the LOCA and LOFA. Some additional sensitivity analysis is performed to examine a specific assumption like the effect of the vacuum vessel initial temperature on the maximum temperature of the rest of the reactor.

Based on the thermal map of the reactor, the inboard FW will radiate a very small amount of heat to the outboard FW, because the temperature difference is small. Thus, the inboard VV is the predominant heat sink available for the inboard components. The massive VV steel structure acts as an immediate heat sink that subsequently heats up. The inboard VV transfers heat by conduction to the top part of the device. Also there is no thermal radiation link between the VV and the magnet structural casing on the inboard side, because of the magnet insulation that prevents thermal leakage during normal operation. Thus, the calculated results are very dependent on the thermal conduction performance of the inboard side of the VV. Heat transfer on the outboard side of the machine is quite different because of the massive steel gate of the maintenance ports that act as a heat sink for both the LOCA and LOFA.

Figure 19 shows the inboard LOFA temperature history of some key components at the midplane. The temperature of the steel inboard vacuum vessel reaches 686¡C after 2.4 days and then decreases with time. The highest temperature in the reactor is at the divertor region and reaches ¯1050¡C after about 2-3 hours. Figure 20 shows the outboard LOFA temperature history of some key components. The temperature of the steel outboard vacuum vessel reaches 474¡C after 14.7 hr and then decreases with time. It is clear that from comparing the two figures

that the inboard is the critical location. Figure 21 illustrates the inboard response to a complete LOCA. The temperature history of the key parts reveals that the temperature in the steel inboard vacuum vessel reaches 636¡C after 3.4 days and then decreases very slowly with time.

The design offers the option of operating the local shield located behind the divertor pumping ducts at the liquid nitrogen temperature (80 K) of the high-temperature TF magnet. In a series of investigations of the effects of the cryoshield on the thermal performance of the reactor components, we assumed that the initial shield temperature could be at the liquid nitrogen temperature (80 K). Figure 22 shows the transient thermal behavior of the inboard side during LOFA, of some key components. The temperature of the inboard vacuum vessel reaches 685¡C after 2.4 days and then decreases with time. Thus, the cryoshield has an insignificant effect on the IB VV peak temperature at the midplane. Table 12 is a summary of the results of LOCA/LOFA analysis assuming different initial conditions. These results show that accident temperatures are within the limits for SiC and ferritic steel structures. Thus, decay heat is removed passively and there is no need for a dedicated separate decay heat removal system for ARIES-AT.

3.4 Chemical Reactivity

The key chemical reactivity issue with the ARIES-AT design is reaction of the blanket coolant with air and water. In terms of LiPb/water interactions, the cooling systems are separate and no credible ex-vessel interactions between LiPb and water have been identified.

The Li in the LiPb is buffered to a large degree by the large heat capacity of the Pb. As a result, reaction with air is not a serious issue in terms of chemical energy production or combustible gas generation as it is with other chemical energy sources under consideration in fusion (e.g., Be/water reactions, Li-water reactions, and Li-air reactions). At temperatures up to 900¡C, no violent reaction was observed in experiments. [18,19] The key concern is the release

of Po-210 and Hg-203 from the LiPb during a spill. As a result, an ex-vessel spill of LiPb coolant in the room housing the coolant manifold was examined to determine the potential for Po-210 and Hg-203 release.[d]

A version of the MELCOR code that simulates coolants other than water, in this case LiPb, was used for this ex-vessel LOCA calculation [20]. The input model described in Section 3.2.1 was extended for this study to include complete one dimensional radial conduction and thermal-radiative heat transfer models of the in-vessel components: first walls, blankets, high temperature shields, and vacuum vessel walls. LiPb coolant volumes for these structures were modeled, including the reentrant coolant flow paths of this coolant inside these components. Steady state flows, MHD pressure drops, and power depositions are from Reference 8. Decay heat is that presented in Section 3.3. The MHD pressure drops are simulated as head loss terms in the liquid momentum equation that varied linearly with fluid velocity, and are applied in the direction of flow. The entire primary heat transport system (PHTS) was modeled, including a pump, piping, accumulator, and heat exchanger. This model represents one quadrant of ARIES-AT, and as such the total LiPb inventory of 150 m^3. The cross-sectional area of the PHTS piping was estimated to be 0.5 m^2. The pumping head required to produce the specified design flow is approximately 3.0 MPa. The major source of flow resistance in this model was not MHD forces (0.18 MPa at 4 m/s flow velocity), but frictional losses in the FW cooling channels.

The selected location for the ex-vessel LOCA to occur was the lower functional areas (LFA). This region of the confinement building is the lowest portion of the building adjacent to the reactor vault, and as such should be the location where the largest spill of coolant for the ARIES-AT design would occur. It was assumed for this event that the LFA was divided into quadrants. An instantaneous double-ended-off-set shear of an outlet coolant pipe at the

[d] Releases of Po-210 and Hg-203 can be mitigated in ARIES-AT through the use of a drain tank system. The drain tank system (one system for each loop) is foreseen for maintenance activities in which the loop must be drained. However, the system could

location it enters the LFA from the reactor vault has been assumed to be the initiator of this accident. The PHTS pump coast down is assumed to occur in 30 seconds. Because the LFA is expected to be a non-nuclear area, the operation of the HVAC system for this area during the accident is the same as that described for the UFA in Section 3.2.

Figure 23 contains the predicted break mass flow rate of LiPb into the LFA following the outlet pipe break. The pipe section connected to the reactor has an initial break flow of about 12,000 kg/s, which decays to 300 kg/s by 200 seconds and to zero by 900 s. The broken section of pipe connected to the PHTS has an initial flow of about 7,000 kg/s. A peak of 15,000 kg/s occurs once the pump stops and the flow in the loop reverses direction. As result of these flows, a 0.238 m deep pool, (with a surface area of 525 m^2 and a total volume of 125 m^3), forms on the floor of the LFA. Figure 24 shows how the temperature of this pool evolves during the course of this accident. The peak temperature is 980¡C, down from the reactor outlet temperature of 1125¡C due to contact cooling of the LiPb with the LFA floor and walls. Because LiPb shows no energetic chemical reaction with air even at 900¡C, chemical reactions will not be a concern for this pool. This figure also shows the concrete floor of the LFA reaching a maximum temperature of 580¡C at 500 seconds. The pool continues to cool until the triple point temperature of LiPb is reached nearly nine hours after the spill occurs. The cooling of the pool is by conduction through the floor and outer wall of the LFA into the ground. It takes two additional days for this pool to completely solidify given these heat transfer assumptions.

For a spill of 150 m^3, 500 Ci of Po-210 and 2.5×10^5 Ci of Hg-203 will be in the pool. Two key processes are involved in the release to the room atmosphere: diffusion from the pool to the pool surface and vaporization off of the pool surface. Diffusion to the pool surface is simply given by: [21]

---

also be used in a spill event if needed to minimize the overall amount of material spilled and the potential for releases to the environment. In the analysis presented here, the effect of the drain tank is not considered to be conservative.

$$FR = 1 - \frac{8}{\pi^2} \sum_{n=0}^{\infty} \frac{1}{(2n+1)^2} \exp[-\frac{D(2n+1)^2 \pi^2}{4L^2}] \quad (1)$$

where

FR = fraction of initial inventory of species that reaches the surface of the pool

D = diffusion coefficient (m^2/s)

L = depth of pool (m).

The diffusion coefficient in the liquid metal can be estimated using the Scheibel modification of the Wilke-Change correlation. [22] It relates diffusivity, D, in cm^2/s to the viscosity of the liquid in Poise ( ), the temperature of the pool in K, and the molar volumes of the species (V_a) and the liquid (V_m) in cm^3/gmole:

$$D(cm^2/s) = 8.2E\text{-}10 [1 + (3V_a/V_m)2/3] T/ [(V_m)^{1/3}] \quad (2)$$

The depth of the pool is ~ 24 cm. For Hg and Po, the values of D range from 1.5×10^{-5} cm^2/s at 200¡C to 1.5×10^{-4} cm^2/s at 1000¡C.

Once at the surface the Hg and Po behave quite differently. The Hg will be well above its boiling point of 360¡C for most of the transient and thus we assume it completely vaporizes once it reaches the surface. For Po, the vaporization is based on an assessment of release data from laboratory experiments as shown in Figure 25. The data are from experiments in Russia, Germany and the US over the past two decades. [23] The line labeled B is a simple vaporization calculation assuming PbPo is the vaporizing species. This line best envelopes the data and was extrapolated to temperatures above 600¡C where no data exist. (The curves for Po and PoO_2 do not adequately predict the trends in the data.) The measured release from the experiments is part aerosol and part vapor. The aerosol is condensed PbPo and vapor is

hydroxide of Po based on RF work. In air some PoO_2 is expected but it decomposes above 500¡C. The experimental results also indicate that more aerosol and less vapor are produced at higher temperatures compared to lower temperatures. Thus, we assume that the release of PbPo is aerosol and we use the vaporization rate recommended by Schipakin:

$$J\ (Ci/cm^2\text{-}hr) = 3.0 \times 10^5\ P_{sat}(T)\ (1000/T)^{0.5}\ [x/x_o]^*\ 1.95 \times 10^{-11} \qquad (3)$$

where $P_{sat}(T)$ is the saturation vapor pressure for PbPo in mm of Hg and the ratio $[x/x_o]$ is a linear correction factor equal to 4.7 to account for the fact the Po concentration in the LiPb in ARIES-AT is 4.7 times higher than the 1.95×10^{-11} mole fraction in Shipakin's experiments. This rate is based on small-scale experiments where there is no limit to transport of PbPo to the surface of the melt. As discussed previously, in the pool there is a significant mass transport resistance to the surface. Thus, for the PbPo, the mass flux of the PbPo arriving at the surface (derivative of Equation 1 converted to mass flux) is compared the rate of vaporization from the surface. The mobilization rate is assumed to be the minimum of these two rates at a given time step in the calculation.

The predicted quantity of Po-210 released as a PbPo aerosol, and the amount of this release that is stacked by the HVAC system to the environment is given in Figure 26. As can be seen, in 17.4 Ci of Po-210 is mobilized, with 11.7 Ci released to the environment prior to isolating the LFA (shutting down the HVAC system) after one hour. Of additional note in Figure 26 is the knee in the mobilization curve after 4000 seconds. This is due to fact that release of PbPo from the pool surface changes from a diffusion-limited bulk process to a surface limited evaporation process. For this pool configuration, the transition occurs at a temperature of 560 ¡C. Figure 27 contains the predicted mobilization of Hg-203 from the spill and stacked to the environment during this accident. In one hour, 8870 Ci are mobilized and nearly 5770 Ci are stacked to the environment. Of this release, 260 Ci is predicted to leak through the walls of the

LFA to the environment before the pool completely solidifies. The quantity of PbPo leaked was negligible. These results are well below the no-evacuation limits. Table 13 summarizes the results of the source term analysis.

4. Waste Management

4.1. Methodology and Limits

The primary options for managing the waste of the ARIES power plants include near-surface disposal as Class A or Class C Low-Level Waste (LLW), recycling and reuse in nuclear facilities, and clearing of materials containing very low radioactivity. Clearance is defined as the unconditional release of materials from radiologically controlled areas after an interim storage period of 50 or 100 years. The emphasis on the approach of disposing, recycling, and clearing the waste differs in various parts of the world. In the U.S., the waste management system offers repositories for both shallow and deep geological burial, for low- and high-level wastes. In Europe, there is no shallow land burial. Thus, the extremely high cost of deep geological disposal drives a strong incentive for recycling and clearance. Compact, high power density machines with well optimized radial builds generating only LLW are being developed in the U.S. with less of an economic and social driver for clearance. On the other hand, relatively larger machines with greater radial builds are designed in Europe [24], emphasizing the recycling and clearance options.

Despite the availability of shallow burial repositories in the U.S., the relatively large volume of waste that fusion generates (~ 0.03 m^3/GWyr) compared to other sources of energy, forces the designers to examine the recycling and clearance options as means to enhance the respository capacity by reducing the volume of solid waste requiring radioactive burial. We applied the disposal and clearance criteria to ARIES-AT. In the past, numerous studies have

addressed the option of recycling and reuse of the waste in nuclear facilities, and readers can consult the references for a broader perspective on this option [25,26,27].

4.1.1. Waste Disposal limits. The Nuclear Regulatory Commission (NRC) defines the waste disposal requirements in the U.S. in 10 CFR 61 [28], which sets specific activity limits for Class A and Class C waste. Class A waste is defined as waste that decays to acceptable levels during the 100 years of assumed institutional control at the disposal site. Because it has a fairly low hazard level, it must meet only the minimum packaging requirements defined in 10 CFR 61. Class C waste must be disposed of 5 m below the surface with engineered intruder barriers, such as concrete covers, to minimize the potential for intruder disturbance of the waste. The NRC waste classification is based largely on radionuclides that are important in fission facilities. In fusion power plants, the isotopes are different because of the different materials being considered and the different transmutation products that are generated. In the early 90 s, Fetter et al. performed analyses to determine the Class C specific activity limits for all long-lived radionuclides of interest to fusion using a methodology similar to that used in 10 CFR 61. Fetter's values have been incorporated into the DOE Fusion Safety Standard [1]. The ARIES approach requires all components meet both NRC and Fetter s limits.

4.1.2. Clearance Limits. During the course of the ARIES studies, we have adopted a national approach for the waste management aspect of the ARIES designs. However, the NRC has not defined the standards for the volumetric contamination that guide the radiation protection program for clearnace of solid materials. On the international level, the development of clearance standards for solids has made a significant improvement over the past several years. In conjunction with various organizations, the International Atomic Energy Agency (IAEA) has developed clearance standards for 1650 radioisotopes of interest to nuclear applications [29] based on a dose limit of 1 mrem/y. Due to the absence of official U.S. guidelines, we have in the interim used the IAEA nuclide-specific clearance limits and applied those limits to the ARIES-AT design.

A unique approach for handling the cleared components has been developed by the ARIES team. At the end of the service lifetime, individual components or constituents will be stored for 100 years, then cleared from regulatory control if the clearance index (CI) is below unity. By definition, the CI is the ratio of the activity (in Bq/kg) to the allowable limit summed over all radioisotopes. Since the ultimate goal is to separate the constituents of the component for recycling and reuse by industry, our approach for handling the cleared components (CI < 1) is to evaluate the CIs at the constituent level. Although the entire component could have a CI < 1, the individual constituents may not, requiring further segregation of the waste based on constituents rather than components. Constituents with CI > 1 will be stored in LLW repositories while cleared solids could be shipped to the industry for recycling.

4.2. Waste Disposal Level

The Fetter s and NRC WDR for the structures of the device are reported in Table 14 at a 100 y after shutdown for fully compacted waste. The main long-lived radionuclides contributing to the WDR are included parenthetically in descending order. The results pertain to a case where the Nb and Mo impurities are controlled to 1 and 20 appm, respectively, in ferritic steel in order to qualify the IB HT shield, in particular, as Class C waste after 40 FPY of operation. Note that Mo and Ag impurities are the main contributors to Fetter's WDR of the W-containing components, namely the OB blanket-II, divertor plate and IB HT shield. Table 14 reveals that almost all components meet the Class C waste disposal requirement by a wide margin. Further segregation of the waste indicates 85% of the ARIES-AT waste volume could qualify as Class A LLW after a 100-year storage period, according to the NRC guidelines. The remaining 15% of the waste that consists of the OB blanket-II + W shells, HT shields, and OB VV would still meet the Class C waste requirements. Table 14 also points out to an interesting difference between the Fetter and NRC Class C WDRs for the SiC FW/B components. The ratio of the OB to IB Class C values is 1.8 for NRC and 4.7 for Fetter. The difference in the ratios is primarily due to

the inclusion of the ^{26}Al radioactive nuclide in the Fetter s limits. The effect of the ^{14}C and ^{26}Al radionuclides on the IB and OB WDR values is not the same. ^{14}C is produced by two successive, low energy reactions with ^{12}C [^{12}C(n,γ)^{13}C(n, γ)^{14}C]. The ratio of the OB to IB NRC Class C values due to ^{14}C is consistent with the ratio of the OB to IB average wall loadings (1.8). The higher Fetter s ratio (4.7) can be explained as follows. More than 95% of the Fetter s Class C WDR is dominated by the ^{26}Al radionuclide. The production of ^{26}Al is from two successive, high energy neutron interactions beginning with the parent nuclide ^{28}Si [^{28}Si(n,np)^{27}Al(n,2n)^{26}Al]. For the ARIES-AT design parameters and operation schedule, a detailed analytical method has shown that, for the same neutron source strength, the ratio of the OB to IB ^{26}Al concentration is approximately 2.7. The corresponding value for ^{14}C is close to one. If we multiply these factors by the ratio of the average wall loadings (1.8), we obtain values of 4.8 and 1.8 which are consistent with the ratios of the OB to IB Fetter s and NRC WDRs, respectively.

Although disposing 5000 ton of LiPb is unpractical, it is illustrative to calculate the WDR of the LiPb breeder/coolant at the end of plant operation. Considering the different flow paths and averaging over all loops, the LiPb WDR value is 4 after 40 FPY of operation. The main contributors are ^{208}Bi (90%) and ^{108m}Ag (10%). A purification system to reduce the Bi inventory to an acceptable level would permit reuse of the LiPb breeder in other fusion devices.

4.3. Clearance Analysis

The clearance index depends strongly on the neutron flux level, spectrum, materials, operation time, and cooling period. Figure 28 illustrates the drop in CI with time after shutdown for the OB components. The IB and divertor components exhibit similar behavior. The CI results at 100 years after shutdown are plotted in Figures 29, 30, and 31 for all components. The OB V.V. has higher CI compared to the HT shield due to the higher VV activity. Re-examining the TF magnet reveals ^{94}Nb is a major contributor (80%) to the CI at a 100 y after shutdown and the silver constituent contributes the remaining 20% although its volume fraction amounts to only

0.5% of the magnet. Note that the magnet employs YBaCuO as a conductor and the Inconel-625 structure of the magnet contains 1.72 wt% Nb as an alloying element. Replacing the Inconel structure by 316 SS would drop the magnet CI by a factor of ~3. The breakdown of the CI is shown in Figure 32 for the winding pack constituents of the outer legs of the magnet. The ^{94}Nb remains the dominant contributor (80-95%) to the magnet CI for times longer than 100y.

Because of the compactness of the machine, CIs for all components exceed the limit by a factor of several hundreds to several thousands. This means the ARIES-AT components cannot be released as cleared metals; therefore, they could either be recycled or disposed near-surface as LLW. An interim analysis indicated that the extra volume of the additional shield required to clear the vacuum vessel and magnet will offset the waste saving and outweighs the benefits [30]. On this basis, no changes have been made to the final design to clear any component by adding more shield to the OB side.

At present, the status of cleared metals in the U.S. is uncertain [30]. The clearance issue is currently the subject of much debate. Extensive discussions and meetings to develop consensus standards have been held with the NRC, Department of Energy, and other organizations. Circumstances may change prior to building a first ARIES power plant in 50 years. Therefore, our approach is not to rule out the clearance option, continue monitoring the clearance level for future ARIES designs, and apply the national NRC clearance standards when released.

4.4. Waste Minimization

During the design process of the ARIES power plants, several measures were taken to reduce the radwaste stream and minimize the volume of the fusion power core (FPC). Those measures include designing high power density machines, optimizing the radial build, segmenting the replaceable components [3], and, eventually, recycling the waste. The outer building surrounding the FPC contains a low level of radioactivity and is likely to be cleared from the waste stream. Figure 33 depicts the evolution of the ARIES waste volume since the

inception of the ARIES project, showing a persistent trend in waste minimization for tokamaks. In comparison with the first ARIES-I design, ARIES-AT demonstrates a factor of two reduction in the FPC volume, which is a significant achievement.

It is informative to compare ARIES-AT with other power plant designs. By optimizing the design to clear its out-of-vessel components, the European design (see Reference 24) calls for a large, low power density machine with greater radial build. The entire ARIES-AT FPC, including the magnet, could fit inside the bore of the EU OB first wall (R= 11.7 m). The EU OB components generate 1600 m^3 of waste (from the blanket, shield, and V.V.) and 500 m^3 of cleared metals (from the magnet). The ARIES-AT OB waste amounts to 500 m^3. A compact device is certainly more attractive than a large machine that generates more waste. Designing a compact machine is a very effective approach to enhance the repository capacity and reduce the waste volume of a fusion system.

5. Summary and Conclusions

ARIES-AT is a 1000 MWe conceptual fusion power plant design with a low projected cost of electricity. The design contains many innovative features to improve both the physics and engineering performance of the system. From the safety and environmental perspective, we have performed a more robust safety analysis than in past ARIES studies. The results indicate that in all cases, the ARIES-AT design can meet the no-evacuation limit assuming conservative on-line removal of Be to 1 ppm. In the area of waste management, both the volume of the component and hazard are used to classify the waste. In comparison to previous ARIES designs, the overall waste volume is less because of the compact design.

REFERENCES

[1] DOE STD 6003-96, The Safety of Magnetic Fusion Facilities, May 1996

[2] G. R. Longhurst, "Tritium Inventory in ARIES-AT," INEEL/EXT-01-00306, February 2001.

[3] L. El-Guebaly, Nuclear performance assessment for ARIES-AT, Fus. Eng. and Des., this issue.

[4] M. Herman and H. Wienke, FENDL/MG-2.0 and FENDL/MC-2.0, the processed cross-section libraries for neutron-photon transport calculations, Report IAEA-NDS-176, International Atomic Energy Agency , March 1997.

[5] DANTSYS: A diffusion accelerated neutral particle transport code system, Los Alamos National Laboratory Report, LA-12969-M, June 1995.

[6] P. Wilson and D. Henderson, ALARA: analytic and Laplacian adaptive radioactivity analysis code technical manual, University of Wisconsin Fusion Technology Institute, UWFDM-1070 (January 1998); http://legacy.ep.wisc.edu/~wilsonp/projects/ALARA/users.guide.html/.

[7] A. Pashchenko et al., FENDL/A-2.0, Neutron Activation Cross-Section Data Library for Fusion Applications, Report IAEA- NDS-173, International Atomic Energy Agency, March 1997.

[8] R. Raffray et al., Fusion power core engineering for the ARIES-AT power plant, Fus. Eng. and Des., this issue.

[9] S. Malang and K. Schleisiek, Dual coolant blanket concept, Kernforschungszentrum Karlsruhe report, KfK 5424, November 1994.

[10] D.K. Sze, E.T. Cheng, and P.H. Wilson, Tritium and polonium control in LiPb, Fus. Eng. and Des., this issue.

[11] S. Malang and R. Mattas, "Comparison of lithium and the eutectic lead-lithium alloy, two candidate liquid metal breeder materials for self-cooled blankets," Fusion Engineering and Design, 27 (1995), p. 399-406.

[12] M. Abbott letter to D. A. Petti, "Revised Results - MACCS2 Doses for Fusion Isotopes

Release to the Atmosphere using P-G Dispersion Parameters," MLA-11-99, April 14, 1999.

[13] H.-W. Bartels, editor, "Accident Analysis Specifications for NSSR-2 (AAS)," version 2, S 81 RI 19 97-05-04 W1.1, SEHD 8.1.C-1, May 6, 1997.

[14] Takase, K., T. Kunugi, and Y. Seki, "Effect of Breach Area and Length to Exchange Flow Rates Under the LOVA Condition in A Fusion Reactor," Fusion Technology, **30**, December 1996

[15] R. M. Summers, et al., "MELCOR 1.8.0: A Computer Code for Severe Nuclear Reactor Accident Source Term and Risk Assessment Analyses," NUREG/CR-5531, Sandia National Laboratories report SAND-90-0364, January 1991.

[16] B.J. Merrill, R.L. Moore, S.T. Polkinghorne, D.A. Petti, "Modifications to the MELCOR code for application in fusion accident analyses," Paper presented at the 5th International Symposium on Fusion Nuclear Technology (ISFNT-5), Rome, Italy, 20 - 24 September 1999, to be published in Fusion Engineering and Design.

[17] ANSYS 5.4 Basic Analysis Procedures Guide. 000856. 2nd Edition, SAS IP, Inc. (1997).

[18] G. Kuhlborsch, F. Reiger, "Physical Properties an Chemical Reaction Behavior of Li17Pb83 Related to Its Use as a Fusion Reactor Blanket Material, Nucl. Eng. Des./Fus. 1 (1984), p. 195-203.

[19] M. Corradini and D.W. Jeppson, "Lithium Alloy Chemical Reactivity with Reactor Materials: Current State of Knowlegde," Fusion Engineering and Design, 14 (1991), p.; 273-288.

[20]. B.J. Merrill, " A Lithium-Air Reaction Model for the MELCOR Code for Analyzing Lithium Fires in Fusion Reactors," Paper presented at the IAEA Technical Committee Meeting on Fusion Safety, F1-TC-1165, Cannes, France, 13-16 June 2000, to be published in Fusion Engineering and Design.

[21] J. Crank, "The Mathematics of Diffusion," Oxford at the Clarendon Press, 1956.

[22] D. A. Powers et. al, "VANESA: A Mechanistic Model of Radionuclide Release and Aerosol Generation During Core Debris Interactions with Concrete," NUREG/CR-4308, July 1986.

[23]O. Schipakin et al., "Experimental study of ^{210}Po release from 17LI-83Pb eutectic," Fusion Engineering and Design, 29 (1995) 164-169.

[24] D. Petti, K. McCarthy, N. Taylor, et al., Re-evaluation of the use of low activation materials in waste management strategies for fusion, Fusion Engineering and Design, 51-52, 435

[25] T. Dolan and G. Butterworth, Vanadium recycling for fusion reactors, Idaho National Engineering and Environmental Laboratory Report, EGG-FSP, 10378 (1994).

[26] Information on U.S. recycling program available at http://www.em.doe.gov/recyc

[27] P. Rocco and M. Zucchetti, Management strategy to reduce the radioactive waste amount in fusion, 6th IAEA Technical Committee Meeting on Developments in Fusion Safety, Naka, Japan (October 1996).

[28] Nuclear Regulatory Commission, 10CFR 61, Licensing requirements for land disposal of radioactive waste, Federal Register, FR47, 57446 (1982).

[29] IAEA, Clearance levels for radionuclides in solid materials — application of exemption principles, Interim Report for Comment, IAEA-TECDOC-855 (1996).

[30] L. El-Guebaly, D. Henderson, A. Abdou, and P. Wilson, Clearance issues for advanced fusion power plants, Proceedings of the ANS 14th Topical on the Technology of Fusion Energy, Park City, Utah, October 2000, to appear.

Table Titles

Table 1. Tritium inventories in ARIES-AT

Component	Inventory from plasma interactions	Inventory from nuclear activation	Total Inventory
First wall	534 g	7 - 8 g	~ 540 g
Divertor	54 g	1 - 2 g	~ 55 g
LiPb Coolant	< 1 g	--	< 1 g
Co-deposited Layers	150 g	---	150 g
Total	711 g	8 - 10 g	~ 745 g
Total Mobilizable in an accident		205 g	

Table 2. Composition of alloying and impurity elements (in wt.%) for ARIES-AT coolant and structures*

Material	$Li_{17}Pb_{83}$	SiC	ORNL FS	W	304 SS	Inconel-625
Density (g/cm^3)	9.58	3.22	7.78	19.35	8.03	8.44
Li	0.7					
C		29.95	0.1	*11	0.08	0.1
N				*20	0.1	
O				*50		
Na		*0.05				
Mg				*10		
Al				*24		0.4
Si		70.05	0.25	*100	0.75	0.5
P					0.045	0.15
S					0.03	0.015
K		*0.18				
Ca				*10		
Sc		*0.013				
Ti						0.4
V			0.025			
Cr		*0.017	9		19	21.5
Mn			0.5	*10	2	0.5
Fe	*10	*0.44	88.055	*75	68.745	5
Co		*0.013	*34			1
Ni	*2	*0.074	*402	*11	9.25	58
Cu		*0.048		*10		
Zn	*10	*0.043				
Ga		*0.005				
As		*0.003				
Se		*0.001				
Br		*0.001				
Rb		*0.001				
Sr		*0.012				
Zr		*0.236				
Nb			*4			1.72
Mo		*0.041	*70	*21		9
Pd			*0.18			
Ag	*5	*0.002	*0.16	*10		
Cd	*5	*0.004	*0.05			
In		*0.001				
Sn	*5	*0.076				
Sb		*0.001				
Cs		*0.001				
Ba		*0.047				
La		*0.018				
Hf		*0.001				
Ta		*0.001	0.07			1.72
W		*0.032	2	99.9638		
Os			*0.02			
Ir		*0.001	*0.05			
Pt		*0.542				
Hg		*0.001				
Pb	99.2925					
Bi	*43		*0.05			
Eu		*0.001	*0.05			
Tb		*0.001				
Dy			*0.05			
Ho			*0.05			
Er			*0.05			
Yb		*0.001				
Th		*0.001				
U		*0.001	*0.6			

* Represents weight part per million (wppm)

Table 3 Dominant radionuclides for activity at various times after shutdown

Time	FW/B	DP+W	HT Shield	V.V.	Magnet
Shutdown	^{28}Al	^{185}W,^{28}Al	^{55}Fe,^{185}W,^{56}Mn	IB: ^{185,187}W,^{186,188}Re OB: ^{187}W,^{55}Fe,^{56}Mn	^{182}Ta,^{110}Ag
t < 1d	^{24}Na,^{31}Si	^{181,185}W	^{55}Fe,^{185,187}W,^{56}Mn	IB: ^{185,187}W,^{186,188}Re OB: ^{187}W,^{55}Fe,^{51}Cr	^{182}Ta,^{58,60}Co
1d < t > 1w	^{24}Na,T,^{32}P	^{181,185}W	^{55}Fe,^{185}W	IB: ^{185}W,^{186}Re OB: ^{55}Fe^{51}Cr	^{182}Ta,^{58,60}Co
1w < t > 1y	T	^{181,185}W	^{55}Fe,^{185}W	IB: ^{185}W OB: ^{55}Fe	^{182}Ta,^{60}Co
1y < t > 10y	T	^{181}W,^{179}Ta	^{55}Fe,T	IB: ^{185}W,^{55}Fe OB: ^{55}Fe	^{60}Co,^{63}Ni
10y < t > 100y	T	T,^{14}C	T,^{63}Ni	IB: ^{63}Ni,^{14}C OB: ^{63}Ni	^{63}Ni
> 100y	^{14}C	^{14}C	^{59}Ni,^{14}C	IB: ^{14}C,^{93}Mo OB: ^{59}Ni	^{94}Nb,^{59}Ni, ^{93}Mo,^{93m}Nb

Table 4. Inventories of Po-210 and Hg-203 in LiPb used in safety analysis

Isotope	Concentration (Ci/m^3)	Inventory
Hg-203	2000	1.2 MCi
Po-210	4.167	2500 Ci

Table 5. Specific activity of dose-dominant isotopes in tungsten

Isotope	Specific Activity (Ci/g)
Ta-182	2.30E-01
W-185	7.89E+00
W-187	3.14E+00
Re-186	8.68E-01
W-181	3.22E+00
Re-184	1.33E-01
Re-188	3.16E-01
Re-184m	2.25E-02
Sc-46	1.14E-03
Sc-48	1.93E-03

Table 6. Radiological Release Targets for ARIES-AT to meet the No-evacuation Objective

	No-evacuation Limit	
	Dose Limit : 10 mSv (1 rem) per off normal event Meteorology : Best-estimate or Average Weather	
Site Boundary	1 km	1 km
Release Point	Ground	Elevated via 100 m stack
Tritium as HTO	150 g	1.3 kg
Activated W dust	6 kg	69 kg
Hg-203	25,000 Ci	250,000 Ci
Po-210	25 Ci	250 Ci

Table 7. Level of radiological confinement needed for different radioactive species in ARIES-AT

Radioactive Species	Mobilizable Inventory	Release Limit	Required Degree of Radiological Confinement
Tritium	180 g	150 g	1.4
W dust	10-100 kg	6 kg	1.6-16
Hg-203	1.2 MCi	25,000 Ci	50
Po-210	2500 Ci	25 Ci	100

Table 8. Source Term Behavior for ARIES-AT LOVA

Material	Mobilizable Inventory	Released to the UFA	Released to the Environment
Tritium	180 g	0.35 g	0.09 g
Dust	10 kg	0.15 g	0.04 g

Table 9. Source Term Behavior for In-vessel LOCA with bypass

Material	Mobilizable Inventory	Released to the Environment
Tritium	205 g-T	7.6 g-T
Dust	10 kg	207 g
Po-210	500 Ci	0.021 Ci
Hg-203	250000 Ci	88.5 Ci

Table 10. Dominant radionuclides for decay heat at various times after shutdown

Time	FW/B	DP+W	HT Shield	V.V.	Magnet
Shutdown	^{28}Al	^{28}Al,^{187}W	^{56}Mn,^{26}Al,^{187}W	IB: ^{187}W,^{188}Re OB: ^{56}Mn,^{187}W	^{182}Ta,^{110}Ag
t < 1d	^{24}Na,^{31}Si	^{185,187}W	Mn^{54,56},^{187}W	IB: ^{185,187}W,^{188}Re OB: ^{187}W,^{56}Mn,^{188}Re	^{182}Ta,^{60}Co
1d < t > 1w	^{24}Na,^{32}P	^{185,187}W,^{182}Ta	^{185,187}W,^{54}Mn,^{59}Fe	IB: ^{185,187}W OB: ^{187}W,^{59}Fe,^{60}Co	^{182}Ta,^{60}Co

Table 11. Average temperature at onset of LOCA/LOFA.

Component	Coolant (¡C)	Structure(¡C)
	Inboard Components	
V.V.	75	100
HT shield	759	806
Blanket	968	925 for side SiC walls
First wall	800	960 for front wall
		925 for back wall
	Outboard components	
Blanket-I: Wall	787	950 for front wall
		925 for back wall
Blanket-I: Channel	965	925 for side SiC walls
Blanket-II: Wall	709	800 for front/back wall
Blanket-II: Channel	932	800 for side SiC walls
HT shield	725	800
VV	75	100

Table 12. Summary of the LOCA and LOFA Results

	Peak temperature in the I/B vacuum vessel at the midplane at stated time (¡C)			
	1 day	2 days	3 days	7 days
$T_{initial}$ = 50¡C				
1 - Complete LOCA (in LiPb and water)	512.3	591.2	611.5	586.3
2 - LOFA in LiPb and LOCA in water	581	665.5	671.9	601.7
$T_{initial}$ = 100¡C				
1 - Complete LOCA (in LiPb and water)	543.8	617.4	634.6	601.5
2 - LOFA in LiPb and LOCA in water	608	683.9	685.9	669.4
3 - LOFA in LiPb and LOFA in water (with cryogenic shield)	607.9	682.2	680.9	590.5

Table 13. Source Term Analysis for Ex-vessel Spill of LiPb

Isotope	Concentration in LiPb (Ci/m3)*	Inventory in Spilled LiPb (Ci)	Amount Mobilized in first two hours(Ci)	Released to the Environment (Ci)
Hg-203	2000	250000	8770	5770
Po-210	4.2	500	17.4	11.7

Table 14. Fetter s and NRC waste disposal ratings at 100 y after shutdown for compacted waste

Limits	Fetter Class C	NRC Class C	NRC Class A
	Inboard Components:		
FW/B	0.019 (^{26}Al,^{14}C)	0.017 (^{14}C)	0.2 (^{14}C)
HT Shield	0.7 (^{94}Nb,^{99}Tc)	0.4 (^{94}Nb)	4.8 (^{94}Nb)
Vacuum Vessel	0.08 (^{99}Tc,^{108m}Ag)	0.008 (^{94}Nb, ^{14}C)	0.08(^{94}Nb, ^{14}C)
Magnet and coil case	0.09 (^{94}Nb,^{99}Tc)	0.07 (^{94}Nb)	0.7 (^{94}Nb)
	Outboard Components:		
FW/B-I	0.09 (^{26}Al,^{14}C)	0.03 (^{14}C)	0.3 (^{14}C)
B-II	0.6 (^{14}C, ^{99}Tc,^{108m}Ag)	0.4 (^{14}C)	4 (^{14}C)
HT Shield	0.2 (^{94}Nb,^{99}Tc)	0.1 (^{94}Nb)	1.4 (^{94}Nb,^{63}Ni)
Vacuum Vessel	0.07 (^{166m}Ho, ^{94}Nb)	0.03 (^{94}Nb,^{63}Ni)	1.7 (^{63}Ni,^{94}Nb)
Magnet and coil case	0.1 (^{94}Nb,^{99}Tc)	0.09 (^{94}Nb)	1.00 (^{94}Nb)
	Divertor Components:		
DP + W coating	0.4 (^{26}Al, ^{108m}Ag)	0.07 (^{14}C)	0.7 (^{14}C)
Manifolds	0.006 (^{26}Al,^{14}C)	0.01 (^{14}C)	0.1 (^{14}C)
Replaceable HT shield	0.2 (^{94}Nb,^{99}Tc)	0.1 (^{94}Nb)	1 (^{94}Nb,^{63}Ni)
HT Shield	0.3 (^{94}Nb,^{99}Tc)	0.2 (^{94}Nb)	2 (^{94}Nb,^{63}Ni)
Vacuum Vessel	0.02 (^{94}Nb,^{99}Tc, ^{166m}Ho)	0.008 (^{94}Nb)	0.1 (^{94}Nb)
Magnet and coil case	0.04 (^{94}Nb, ^{99}Tc)	0.03 (^{94}Nb)	0.3 (^{94}Nb)

Figure Captions:

Figure 1. Inboard activity results.

Figure 2. Outboard activity results.

Figure 3. Divertor activity results.

Figure 4. ^{209}Bi and ^{210}Po inventories.

Figure 5 Mercury inventories in LiPb.

Figure 6. ARIES-AT Vacuum vessel pressure during a LOVA

Figure 7. ARIES-AT bypass duct flow during initial 2000 seconds of a LOVA

Figure 8. ARIES-AT VV pressure during a LOVA

Figure 9. Dust in upper functional area and stacked to the environment during a LOVA in ARIES-AT.

Figure 10. Pressure response to in-vessel LOCA with bypass in ARIES-AT.

Figure 11. Liquid and vapor mass in the plasma chamber during the first 4000 seconds of the transient.

Figure 12. Mass flow rate from the plasma chamber during the upper functional area

Figure 13. Mass flow rates from the VV to the plasma chamber and from the plasma chamber to the suppression tank.

Figure 14. Inboard decay heat results.

Figure 15. (a) Outboard decay heat results. (b) A representative detailed decay heat plot for the OB FW, channel and backwall of the FW/Blanket-I. Similar data was provided to the LOCA/LOFA analysis for all other components.

Figure 16. Divertor decay heat results.

Figure 17. FW/Blanket and LiPb decay heat comparison.

Figure 18. Finite-element model.

Figure 19. Inboard LOFA temperature history of some key components.

Figure 20. Outboard LOFA temperature history of some key components.

Figure 21. Inboard LOCA temperature history of some key components.

Figure 22. Inboard LOFA temperature history of some key components with cryogenic shield starts at 80 K.

Figure 23. Break mass flow rates during an ex-vessel LOCA in ARIES-AT

Figure 24. Coolant spill temperatures during an ex-vessel LOCA in ARIES-AT.

Figure 25. Experimental measurements of the release of Po from LiPb andPbBi melts compared with simple vaporization of different species

Figure 26. Po-210 release during an ex-vessel LOCA in ARIES-AT

Figure 27. Hg-203 release during an ex-vessel LOCA in ARIES-AT

Figure. 28. Reduction of clearance index with time after shutdown due to the decay of radionuclides

Figure 29. Clearance indices for inboard components evaluated at 100 years after shutdown

Figure 30. Clearance indices for outboard components evaluated at 100 years after shutdown

Figure 31. Clearance indices for divertor components evaluated at 100 years after shutdown

Figure 32. Contribution of individual constituents to the clearance index of outboard TF magnet. (The Inconel, conductor, silver, CeO_2 insulator, and polyimide insulator occupy 72, 7, 0.5, 7, and 13.5% of the magnet volume.)

Figure 33. Volume of waste generated by the various ARIES designs (volumes are not compacted and replaceable components are not included)

Figure 1

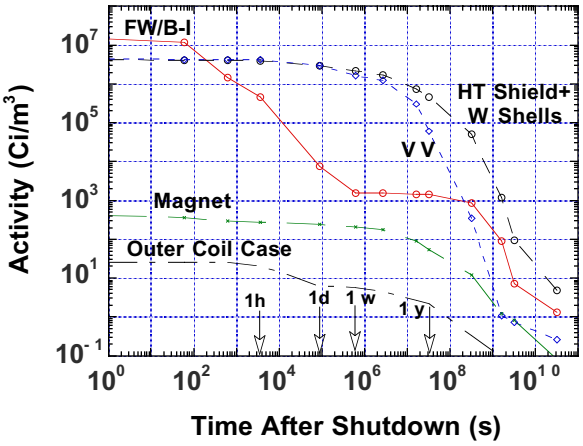

Figure 2

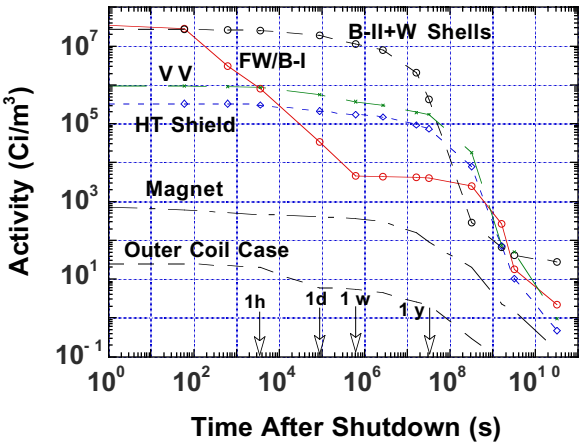

Figure 3

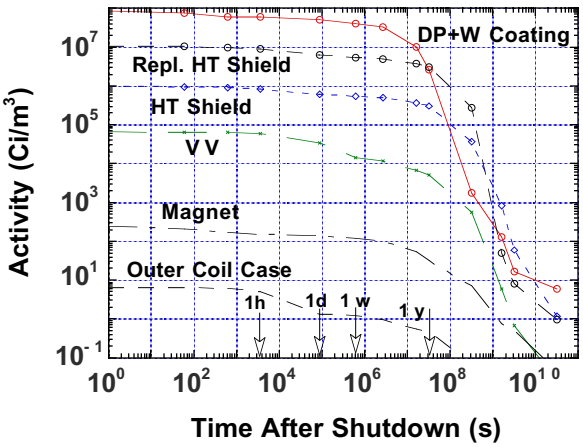

Figure 4

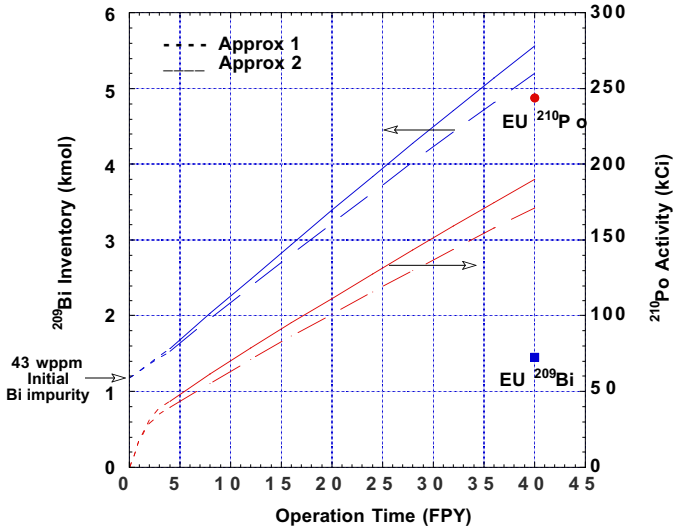

Figure 5

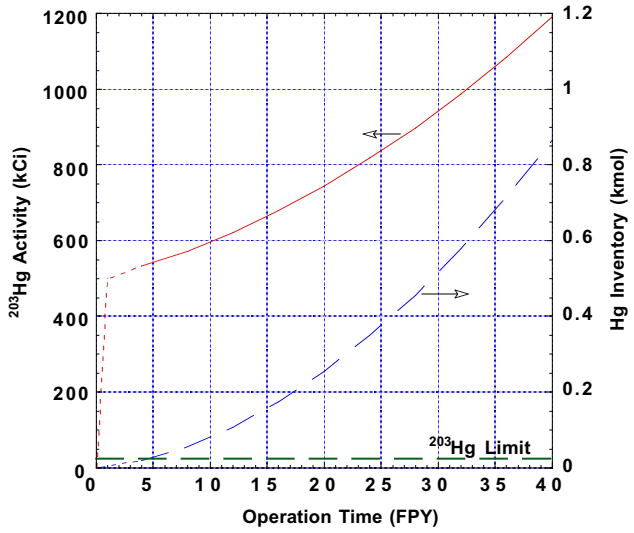

Figure 6

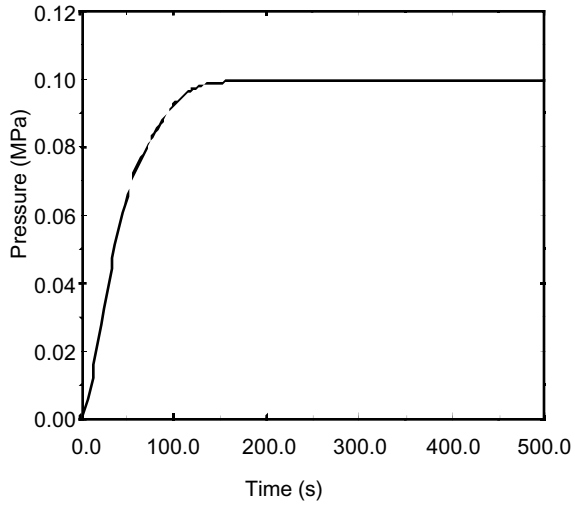

Figure 7

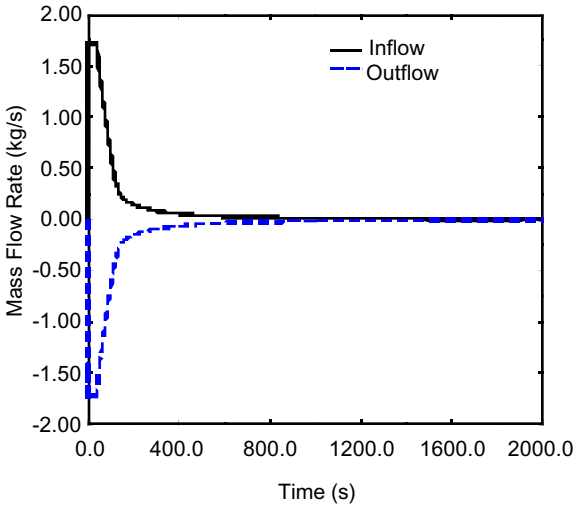

Figure 8

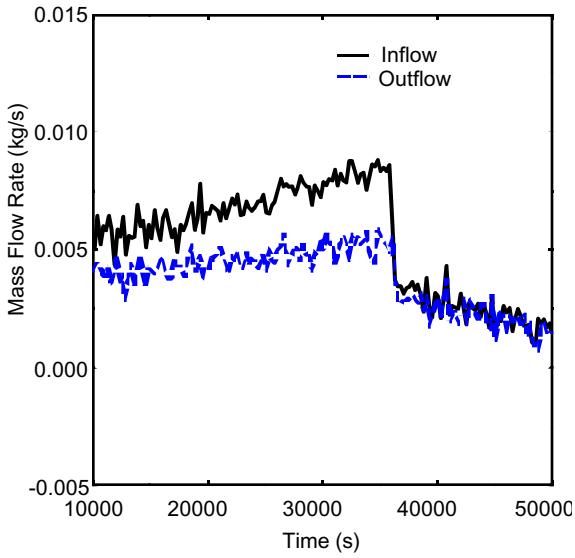

Figure 9

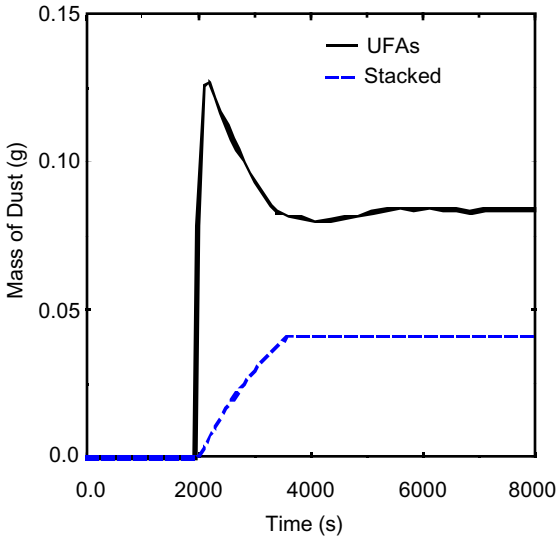

Figure 10

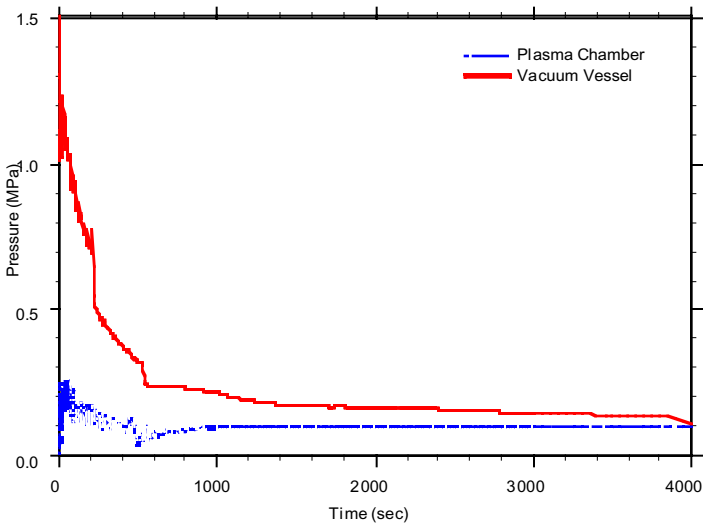

Figure 11

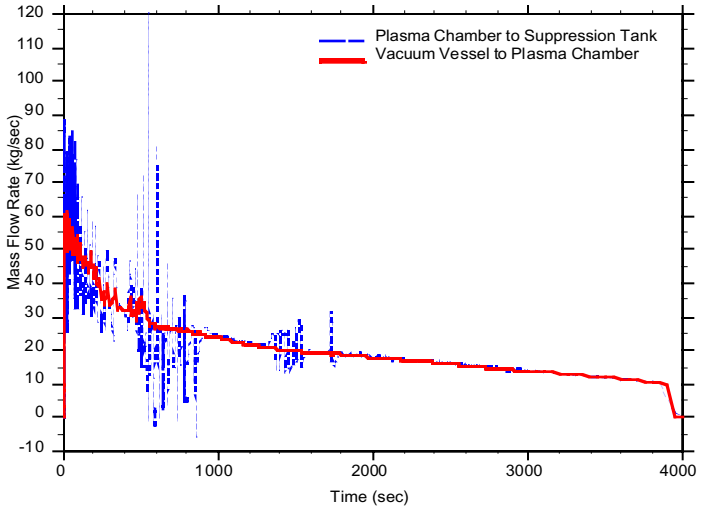

Figure 12

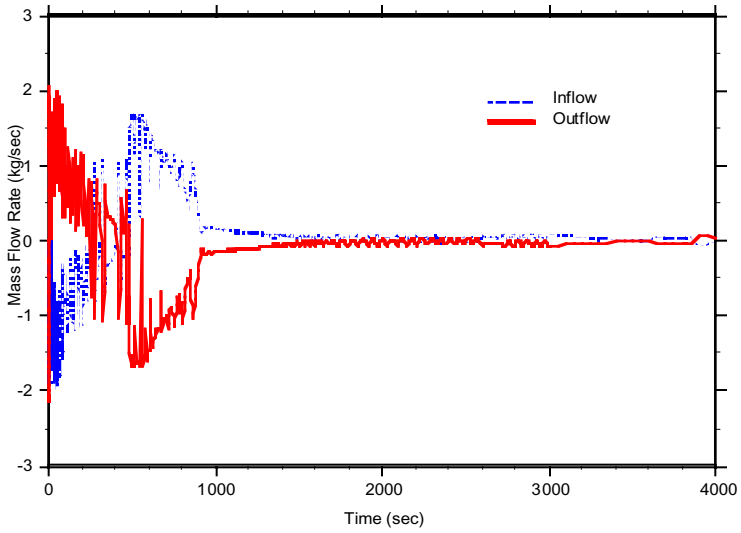

Figure 13

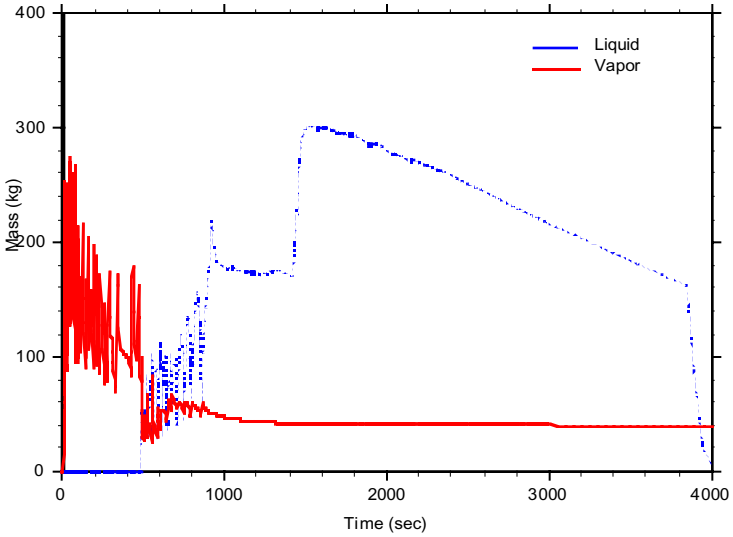

Figure 14

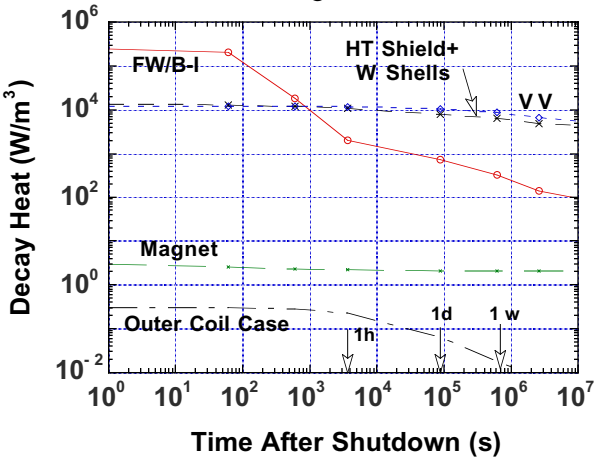

Figure 15a

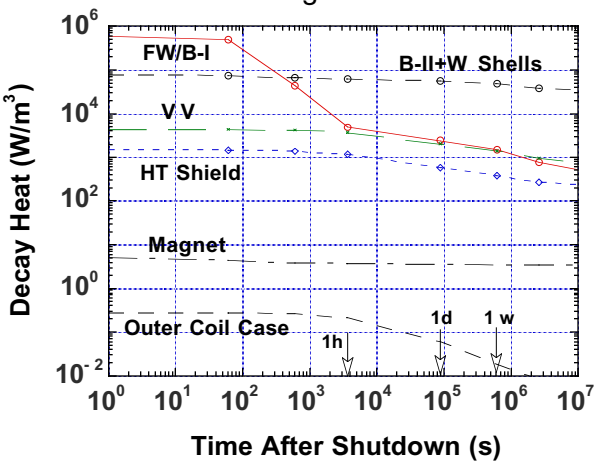

Figure 15 b

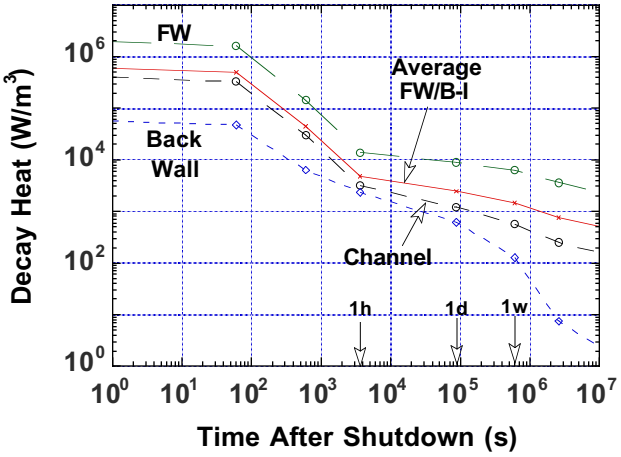

Figure 16

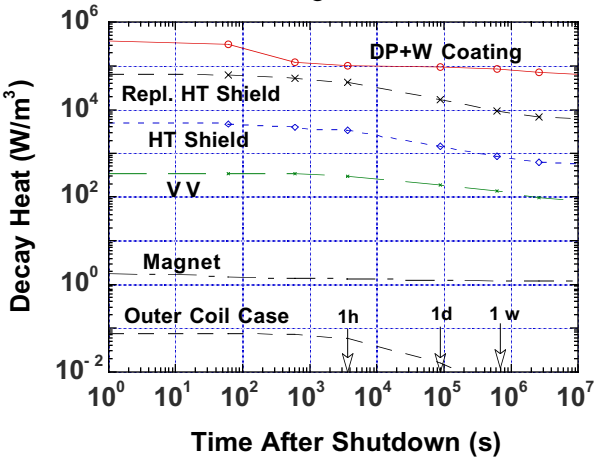

Figure 17

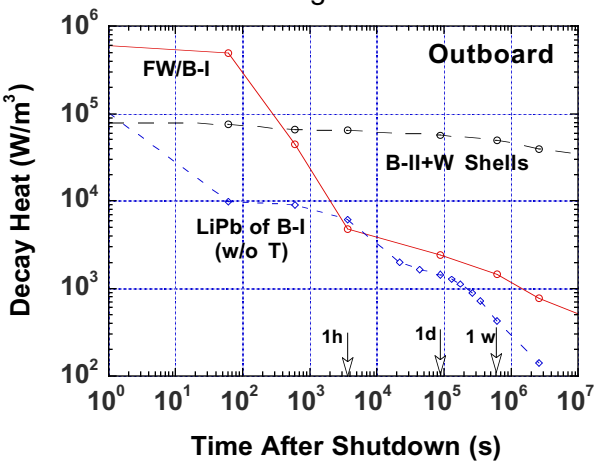

Figure 18

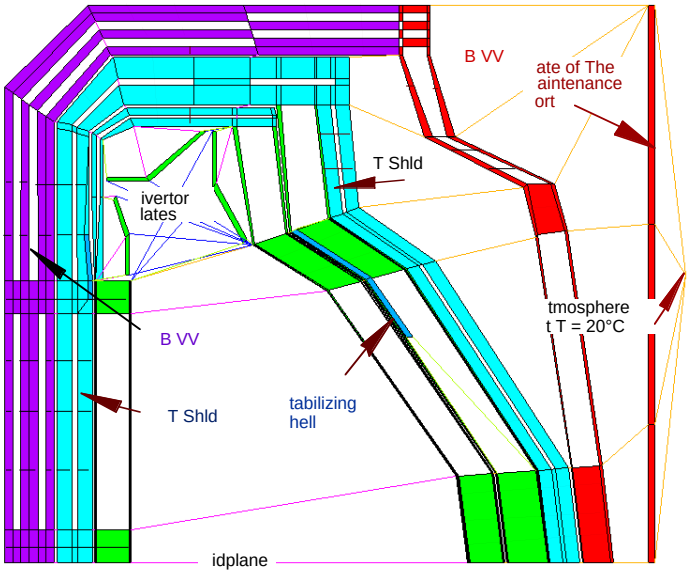

Figure 19

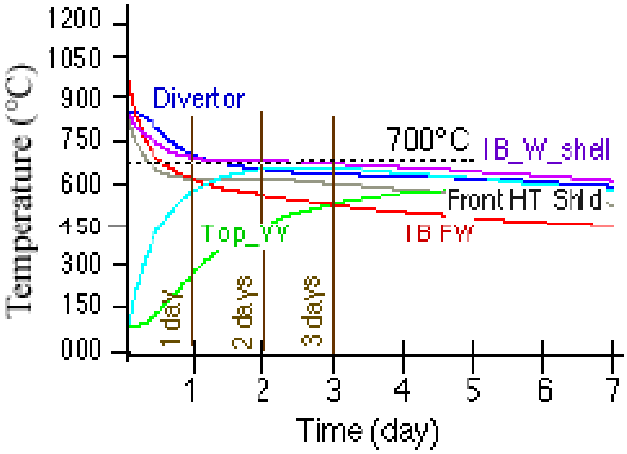

Figure 20

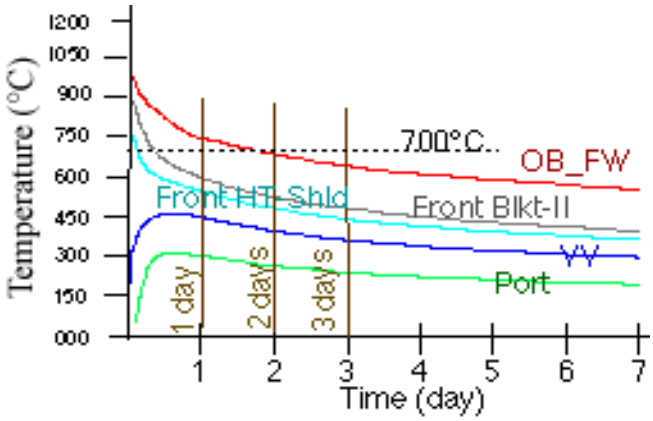

Figure 21

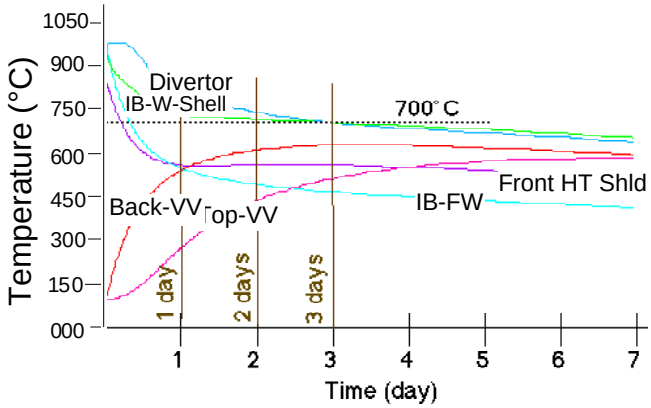

Figure 22

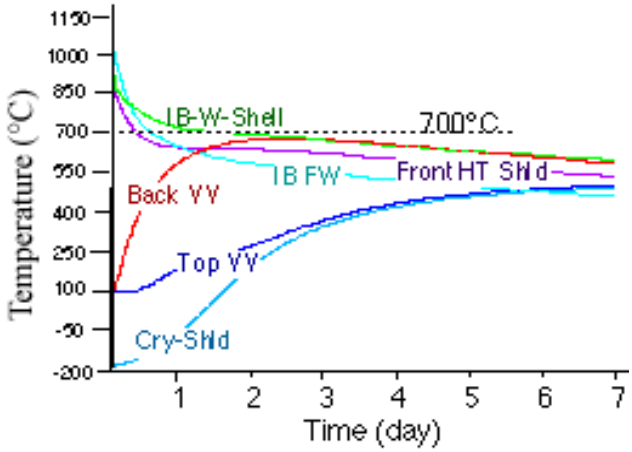

Figure 23

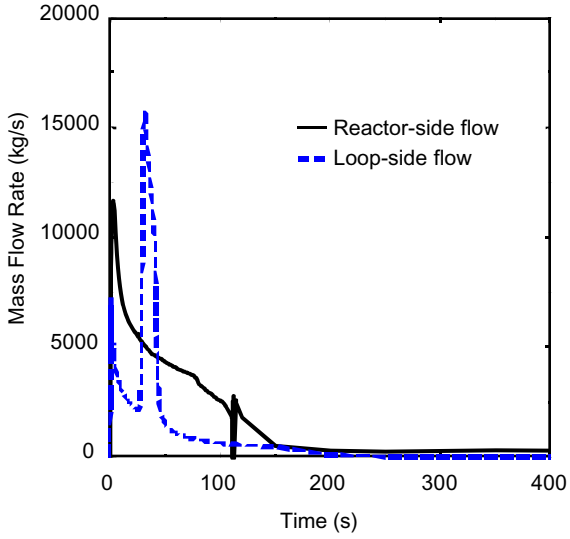

Figure 24

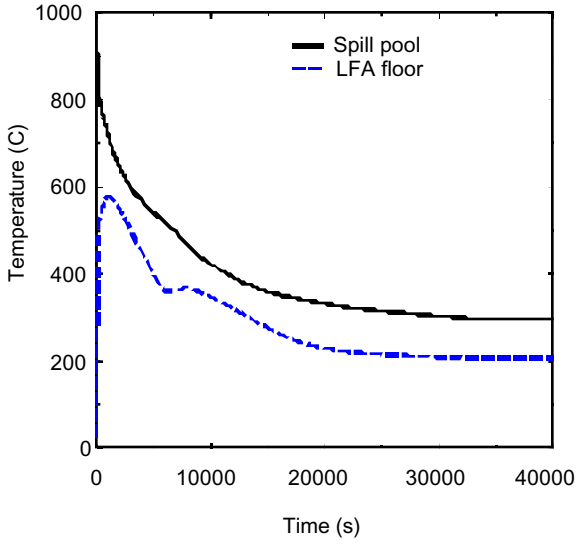

Figure 25

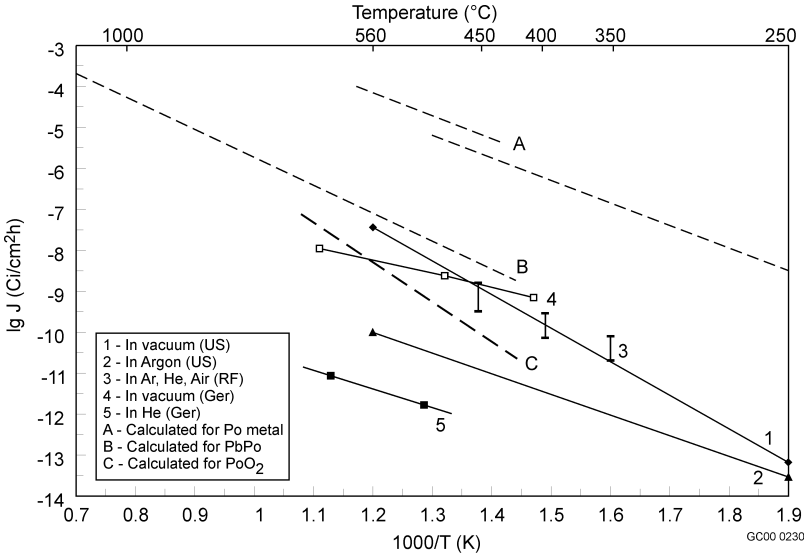

Figure 26

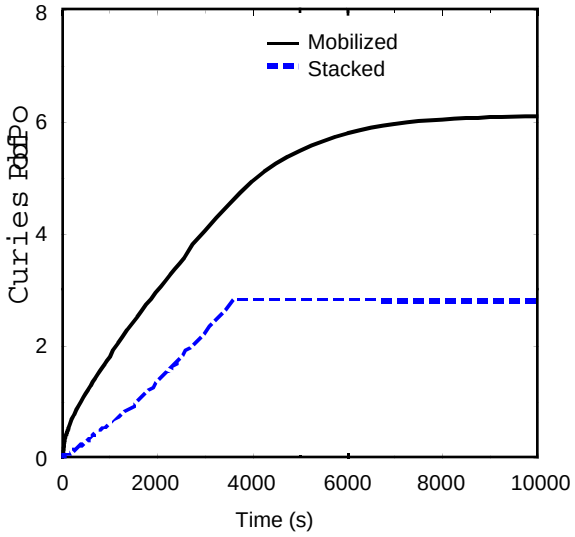

Figure 27

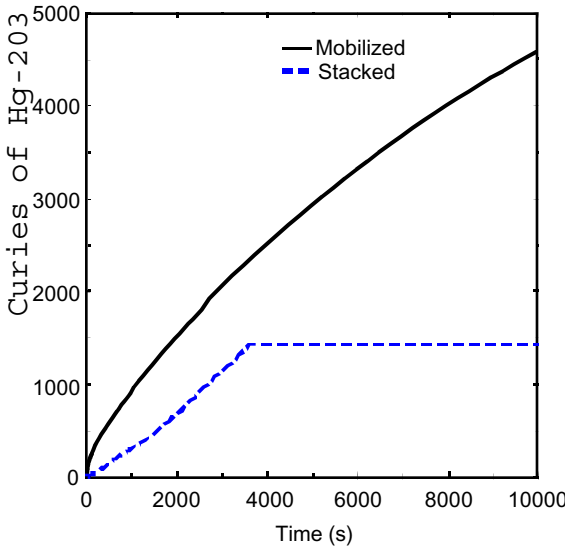

Figure 28

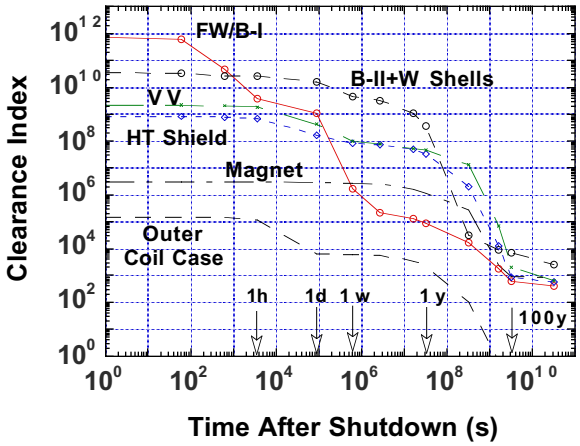

Figure 29

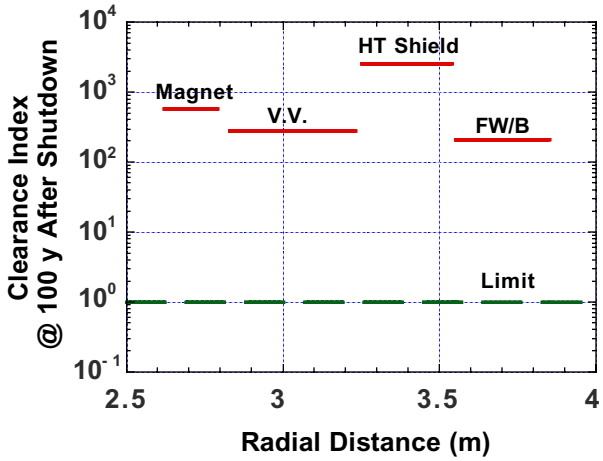

Figure 30

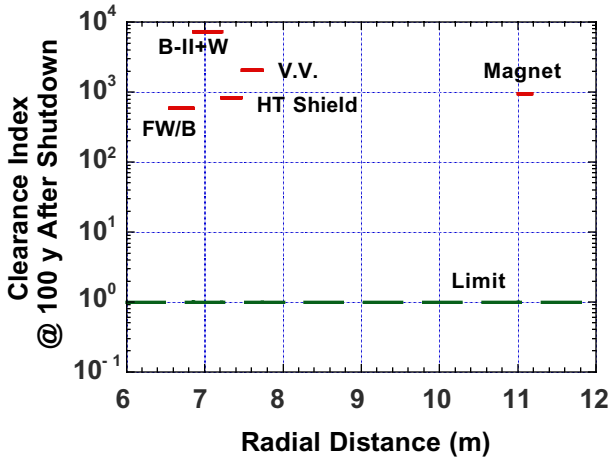

Figure 31

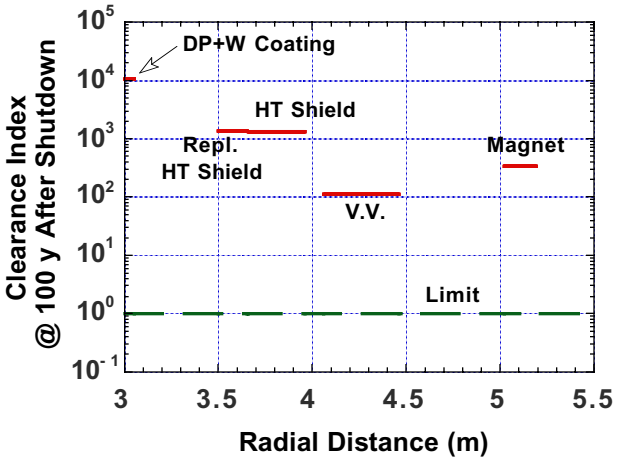

Figure 32

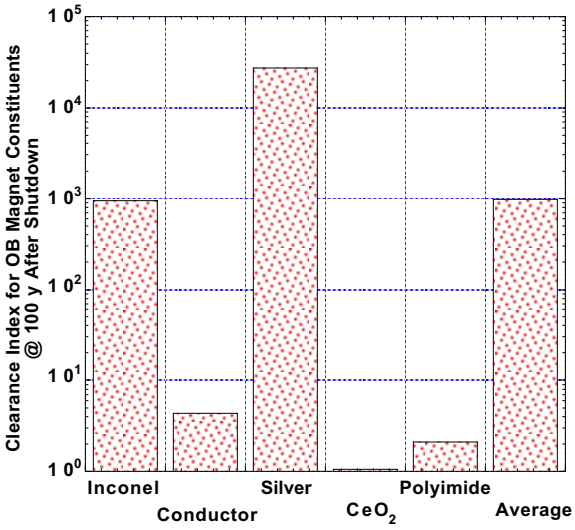

Figure 33

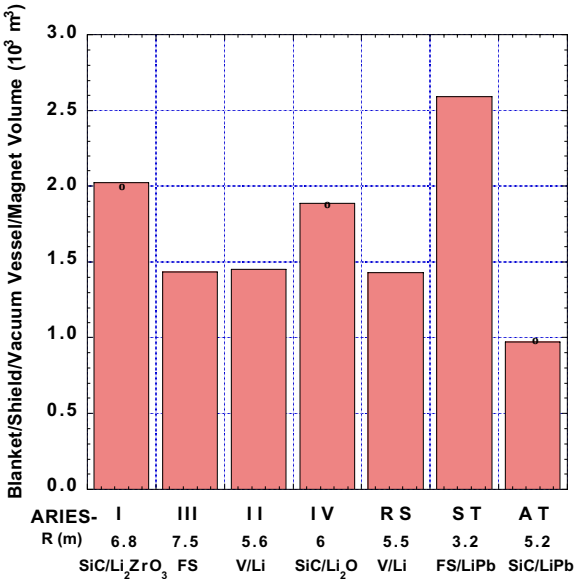
Blanket/Shield/Vacuum Vessel/Magnet Volume (10^3 m^3)
3.0
2.5
2.0
1.5
1.0
0.5
0.0
ARIES-
R (m)
SiC/Li_2ZrO_3
I
6.8
III
7.5
FS
II
5.6
V/Li
IV
6
SiC/Li_2O
RS
5.5
V/Li
ST
3.2
FS/LiPb
AT
5.2
SiC/LiPb